

# A strategy to search for an inner binary black hole from the motion of the tertiary star I: a perturbative analytic approach to a coplanar and near-circular three-body system and its application to 2M05215658+4359220

Toshinori Hayashi,<sup>1</sup><sup>★</sup> Shijie Wang,<sup>1</sup> and Yasushi Suto<sup>1,2</sup>

<sup>1</sup>*Department of Physics, The University of Tokyo, Tokyo, 113-0033, Japan*

<sup>2</sup>*Research Center for the Early Universe, School of Science, The University of Tokyo, Tokyo, 113-0033, Japan*

Accepted XXX. Received YYY; in original form 2018 October 27

## ABSTRACT

There are several on-going projects to detect a number of stars orbiting around invisible objects. A fraction of them may be a triple system consisting of an inner binary black hole (BBH) and an outer orbiting star. In this paper, we propose a methodology to search for a signature of the inner BBH, possibly a progenitor of gravitational wave sources recently detected by *LIGO*, from the precise radial velocity follow-up of the outer star. For simplicity and definiteness, we focus on a coplanar and near-circular three-body system and derive analytic perturbation formulae of the orbital elements for the outer star. This formula will be useful in designing a follow-up radial velocity observation to search for an invisible BBH. As a specific example, we consider the 2M05215658+4359220 system of a red giant orbiting around an unseen object. The resulting constraint reveals that if the unseen companion is indeed a BBH of roughly equal masses, its orbital period should be less than a couple of weeks. Future radial-velocity monitoring of the system for a week will either strengthen the constraint or even detect a signature of the inner BBH. A similar velocity modulation, however, may be produced by a planet around the outer star as well. Thus we consider the degeneracy between the inner BBH and planet-star interpretations as well. In either case, short-cadence follow-up monitoring of a star-black binary system in future offers an interesting possibility to search for otherwise invisible BBHs.

**Key words:** celestial mechanics – techniques: radial velocities – binaries: close

## 1 INTRODUCTION

The first direct detection of a gravitational wave (GW) from a binary black-hole (BBH) merger (Abbott et al. 2016) has convincingly established the presence of very compact BBHs in the universe. The origin, evolution and distribution of such BBHs are hardly understood, but several interesting scenarios have been proposed so far. The binary evolution scenario (e.g. Belczynski et al. 2002, 2007, 2012, 2016; Dominik et al. 2012, 2013; Kinugawa et al. 2014, 2016; Spera et al. 2019) considers that massive stars like Pop III stars are formed as binary systems, experience supernovae, and finally evolve into compact binaries including binary black holes. The dynamical formation scenario (e.g. Portegies Zwart & McMillan 2000; O’Leary et al. 2009; Rodriguez et al. 2016; Tagawa et al. 2016) considers that black holes in dense star clusters experience significant gravitational interactions and binary black holes can be formed due to the occasional capture. The primordial origin scenario (e.g. Sasaki et al. 2016, 2018; Bird et al. 2016) proposes that numerous primordial black holes are formed in the very early universe and they finally interact each other and form binary black holes through GW emission.

<sup>★</sup> E-mail: hayashi@utap.phys.s.u-tokyo.ac.jp

Regardless of such different formation scenarios, however, there should be abundant progenitor BBHs with wider separations and thus longer orbital periods. Detection of such unseen wide-separation BBHs is very challenging, but if successful, it will not only constrain the formation and evolutionary channel towards the GW emitting BBHs, but also establish a yet unknown class of exciting astrophysical objects.

Those BBHs do not generate a detectable GW signal until a few seconds before the final merger. Also they are difficult to be detected directly unless they are surrounded by appreciable accretion disks. Therefore, the presence of such unseen binaries have to be searched for through their dynamical influence on nearby visible objects.

Indeed there exist a couple of interesting systems that are relevant for such a strategy. One is a triple system consisting of a white dwarf-pulsar binary and an outer white dwarf orbiting around the inner binary (Ransom et al. 2014). The system was detected with the arrival time analysis of the pulsar. Quite interestingly, the inner and outer orbits of the triple system are near-circular and coplanar; the eccentricities of the inner and outer orbits are  $e_{\text{in}} \sim 6.9 \times 10^{-4}$  and  $e_{\text{out}} \sim 3.5 \times 10^{-2}$ , and their mutual inclination is  $i = (1.20 \pm 0.17) \times 10^{-2}$  deg.

The other is a red giant 2M05215658+4359220 with an unseen massive object, possibly a black hole (Thompson et al. 2018). The system was discovered from a systematic survey of stars exhibiting anomalous accelerations. The follow-up radial-velocity (RV) observation indicates that the orbit is also near-circular;  $e_{\text{out}} = 0.00476 \pm 0.00255$ .

The two examples are very encouraging, implying that the dynamical search for unseen companions of visible objects is very rewarding, and even that a near-circular outer binary with a near-circular and coplanar inner binary really exists.

Furthermore there are several on-going/future projects that search for unseen companions around stars. *Gaia* was launched at the end of 2013, and is performing astrometric survey for a billion of stars in the Galaxy. Since the astrometry of *Gaia* has great astrometric precision especially for bright stars, it can detect a subtle motion of a star around an unseen object. Therefore, in addition to the survey of stellar binaries (e.g. El-Badry & Rix 2018; Ziegler et al. 2018), there are many proposals to search for star – black hole binaries with *Gaia* (e.g. Breivik et al. 2017; Kawanaka et al. 2017; Mashian & Loeb 2017; Yamaguchi et al. 2018). Yamaguchi et al. (2018), for instance, estimate that *Gaia* can detect 200 – 1000 binaries in its 5 year operation.

*TESS* launched in 2018 is carrying out a photometric survey of near-by stars to search for transit planets. Masuda & Hotokezaka (2018) conclude that *TESS* will potentially discover  $\sim 10^3$  binaries consisting of a star and an unseen compact object through identifying a relativistic effect in their photometric light-curves.

Thus it is quite likely that *Gaia*, *TESS* and other surveys detect numerous binary systems with an unseen object. Given the LIGO discovery of very tight BBHs, it is natural to expect that a fraction of those systems are indeed triple systems that host unseen inner BBHs. Therefore it is important to see if one can dynamically distinguish between a single black hole and a binary black hole in such triple systems. In addition, the stellar evolution of multiple systems is still poorly understood. Toonen et al. (2016) do a pioneering systematic work theoretically on the stellar evolution of triples. The detection of triples with inner BBHs will contribute to understand various processes during the evolution of multiples.

In this paper, we propose a methodology to search for an inner BBH in a triple system from the short-term outer stellar RV variations (Figure 4) due to inner binary perturbation (Figure 2) in an overall RV curve (Figure 3) through intensive RV monitoring for a short period. For that purpose, we consider the orbital evolution of an outer visible body in a near-circular and coplanar triple system. While this is a fairly idealized system, there exists at least one system as we mentioned in the above. Also such a system allows us to approach the problem analytically by applying a perturbation theory established in the hierarchical three-body problem. This provides a good physical insight on the dynamical behavior of such systems, and also puts preliminary constraints on the parameter space before performing an intensive numerical study to unambiguously identify the inner BBHs from the observational campaign. The approximation formulae derived here will be also helpful in designing the RV follow-up properly.

As the first part of a series, this paper (part I) concentrates on the methodology and idea to search for a BBH through an analytic approach. The feasibility check using numerical simulations and practical analysis will be discussed in the second paper (part II). The rest of the paper is organized as follows. Section 2 briefly reviews the formulation of the three-body problem that we adopted here, and derives the basic perturbation equations. We solve the equations perturbatively in Section 3 and propose a methodology to search for compact binaries schematically using the solutions. Section 4 applies our analytic solutions to the binary system 2M05215658+4359220 (Thompson et al. 2018), and constrains the mass ratio and the orbital period of a possible inner binary. We also examine the validity of the analytic result against numerical simulations. If the outer star is accompanied by a planet, the star exhibits a RV modulation similar to that induced by an inner BBH. We discuss the degeneracy between the two pictures, and derive the parameter correspondence in section 5. Finally, section 6 is devoted to the summary of this paper. Appendix A examines the validity of the approximate analytic solution against the numerical simulations.

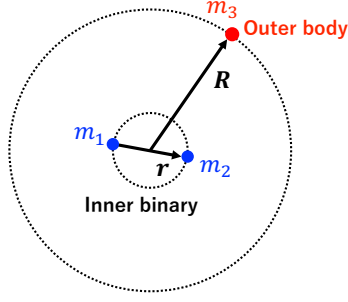


**Figure 1.** Schematic illustration of a coplanar and near-circular triple system. The relative position vectors  $\mathbf{r}$  and  $\mathbf{R}$  are defined in the Jacobian coordinate.

symbol	meaning
$\mathbf{r}_i (i = 1, 2, 3)$	position vector of $m_i (i = 1, 2, 3)$ in arbitrary reference frame
$\mathbf{r} \equiv \mathbf{r}_2 - \mathbf{r}_1$	position vector of inner orbit in Jacobian coordinate system
$\mathbf{R} \equiv \mathbf{r}_3 - \frac{m_1 \mathbf{r}_1 + m_2 \mathbf{r}_2}{m_{12}}$	position vector of outer orbit in Jacobian coordinate system
$m_{12} \equiv m_1 + m_2$	total mass of inner binary
$m_{123} \equiv m_1 + m_2 + m_3$	total mass of system
$\mu_{\text{in}} \equiv m_1 m_2 / m_{12}$	reduced mass of inner binary
$\mu_{\text{out}} \equiv m_3 m_{12} / m_{123}$	reduced mass of three-body system
$a$	semi-major axis
$\alpha \equiv a_{\text{in}} / a_{\text{out}}$	semi-major axis ratio; after Section 3, $\alpha \equiv a_{\text{in}}^{(i)} / a_{\text{out}}^{(i)}$
$\epsilon$	instantaneous mean longitude at epoch
$\lambda \equiv \int_0^t \nu dt' + \epsilon$	mean longitude
$\Omega$	longitude of the ascending node
$\omega$	argument of pericentre
$\varpi \equiv \omega + \Omega$	longitude of pericentre
$e$	eccentricity
$h \equiv e \sin \varpi$	
$k \equiv e \cos \varpi$	
$\nu_{\text{in}} \equiv \sqrt{G m_{12} / a_{\text{in}}^3}$	mean motion of inner binary
$\nu_{\text{out}} \equiv \sqrt{G m_{123} / a_{\text{out}}^3}$	mean motion of outer body

**Table 1.** Definitions of major variables in the present analysis.

## 2 COPLANAR AND NEAR-CIRCULAR HIERARCHICAL THREE-BODY SYSTEM

Figure 1 illustrates a schematic configuration of a hierarchical three-body system that we consider in the present paper. An outer body of mass  $m_3$  is orbiting around an unseen inner binary of masses  $m_1$  and  $m_2$ , and both orbits are near-circular on a coplanar plane.

We use the Jacobian coordinate, and write down the basic equations since the Jacobian coordinates separates well the Keplerian motions from the perturbation terms. Standard three-body perturbation theories are described in many textbooks of celestial mechanics including, *e.g.*, Moulton (1914), Danby (1988) and Murray & Dermott (2000). Specifically, we adopt the formulation of Mardling (2013). Major variables adopted in this paper are summarized in Table 1 for clarity.

### 2.1 Basic formulation of the Lagrange planetary equations

Equations of motion for the inner and outer orbits in Figure 1 are given by

$$\mu_{\text{in}} \ddot{\mathbf{r}} + \frac{G m_1 m_2}{r^3} \mathbf{r} = \frac{\partial \mathcal{R}}{\partial \mathbf{r}} \quad (2.1)$$

and

$$\mu_{\text{out}} \ddot{\mathbf{R}} + \frac{G m_{12} m_3}{R^3} \mathbf{R} = \frac{\partial \mathcal{R}}{\partial \mathbf{R}}, \quad (2.2)$$

where  $\mathbf{r}$  and  $\mathbf{R}$  are position vectors of the inner and outer orbits, respectively, in terms of the Jacobian coordinates, and we define  $r = |\mathbf{r}|$ ,  $R = |\mathbf{R}|$ ,  $m_{12} = m_1 + m_2$ ,  $\mu_{\text{in}} = m_1 m_2 / m_{12}$ ,  $\mu_{\text{out}} = m_{12} m_3 / m_{123}$ , and  $m_{123} = m_1 + m_2 + m_3$ .

The disturbing function  $\mathcal{R}$  in equations (2.1) and (2.2) is explicitly written as

$$\mathcal{R} = -\frac{Gm_1m_3}{R} + \frac{Gm_2m_3}{|\mathbf{R} - (m_1/m_{12})\mathbf{r}|} + \frac{Gm_1m_3}{|\mathbf{R} + (m_2/m_{12})\mathbf{r}|}. \quad (2.3)$$

According to [Mardling \(2013\)](#), this disturbing function for a coplanar case can be written explicitly as an infinite series of cosine functions:

$$\mathcal{R} = \sum_{m=0}^{\infty} \sum_{n=-\infty}^{\infty} \sum_{n'=-\infty}^{\infty} \mathcal{R}_{mnn'} \cos \phi_{mnn'}. \quad (2.4)$$

In what follows, we use two subscripts {in,out} to indicate the inner and outer orbits, respectively. The coefficients of the disturbing function in the right-hand-side of equation (2.4) are further expanded as

$$\mathcal{R}_{mnn'} = \frac{G\mu_{in}m_3}{a_{out}} \sum_{l=l_{min},2}^{\infty} \zeta_m c_{lm}^2 \mathcal{M}_l \alpha^l X_n^{l,m}(e_{in}) X_{n'}^{-(l+1),m}(e_{out}), \quad (2.5)$$

where the above summation over  $l$  is performed in steps of two from  $l_{min}$ :

$$l_{min} \equiv \begin{cases} 2, m = 0 \\ 3, m = 1 \\ m, m \geq 2 \end{cases}. \quad (2.6)$$

The arguments of the cosine function in equation (2.4) are given as

$$\phi_{mnn'} \equiv n\lambda_{in} - n'\lambda_{out} + (m-n)\varpi_{in} - (m-n')\varpi_{out}, \quad (2.7)$$

where  $\lambda$  is the mean longitude and  $\varpi$  is the longitude of pericentre. Also the coefficients  $X_n^{l,m}(e_{in})$  and  $X_{n'}^{-(l+1),m}(e_{out})$  in equation (2.5) are called the Hansen coefficients (see [Mardling 2013](#), for further details) and defined as

$$X_n^{l,m}(e_{in}) \equiv \frac{1}{2\pi} \int_0^{2\pi} \left(\frac{r}{a_{in}}\right)^l e^{imf_{in}} e^{-inM_{in}} dM_{in} \quad (2.8)$$

and

$$X_{n'}^{-(l+1),m}(e_{out}) \equiv \frac{1}{2\pi} \int_0^{2\pi} \left(\frac{R}{a_{out}}\right)^{-(l+1)} e^{-imf_{out}} e^{in'M_{out}} dM_{out}, \quad (2.9)$$

where  $f$  is the true anomaly,  $M$  is the mean anomaly,  $e$  is the eccentricity, and  $a$  is the semi-major axis.

The other coefficients in equation (2.5) are defined as

$$\alpha \equiv a_{in}/a_{out}, \quad c_{lm} \equiv \sqrt{\frac{8\pi}{2l+1}} Y_{lm}(\pi/2, 0), \quad \mathcal{M}_l \equiv \frac{m_1^{l-1} + (-1)^l m_2^{l-1}}{m_{12}^{l-1}}, \quad \zeta_m \equiv \begin{cases} 1/2, m = 0 \\ 1, m \neq 0 \end{cases}. \quad (2.10)$$

We note that  $\mathcal{M}_2$  does not show up explicitly in the following expressions simply because  $\mathcal{M}_2 = 1$  from the above definition.

The Lagrange planetary equations for the orbital elements in terms of the disturbing function  $\mathcal{R}$  reduce to

$$\frac{da}{dt} = \frac{2}{\mu\nu a} \frac{\partial \mathcal{R}}{\partial \lambda} \quad (2.11)$$

and

$$\frac{d\epsilon}{dt} = -\frac{2}{\mu\nu a} \left(\frac{\partial \mathcal{R}}{\partial a}\right)_{\nu, \text{fixed}} + \frac{\sqrt{1-e^2} (1 - \sqrt{1-e^2})}{\mu\nu a^2 e} \frac{\partial \mathcal{R}}{\partial e}, \quad (2.12)$$

where we define  $\epsilon$  as the instantaneous mean longitude at epoch. Note that the  $\epsilon$  has the following relation:

$$\lambda \equiv \int_0^t \nu dt' + \epsilon. \quad (2.13)$$

This relation reduces to a famous relation  $\lambda = \nu t + \epsilon$  for a two-body problem. Later, we see that the secular growth of  $\epsilon$  adds a tiny correction to the Keplerian orbital frequency.

The Lagrange planetary equations for  $e$  and  $\varpi$  include apparent divergent terms for near-circular cases that we consider here. In order to remove the apparent divergence, we introduce the following two variables:

$$h \equiv e \sin \varpi, \quad k \equiv e \cos \varpi. \quad (2.14)$$

Then the equations of motion for  $e$  and  $\varpi$  are replaced by

$$\dot{h} = \frac{1}{\mu a^2 \nu} \sqrt{1-e^2} \frac{\partial \mathcal{R}}{\partial k} - \frac{h}{\mu a^2 \nu} \frac{\sqrt{1-e^2}}{1 + \sqrt{1-e^2}} \frac{\partial \mathcal{R}}{\partial \epsilon}, \quad \dot{k} = -\frac{1}{\mu a^2 \nu} \sqrt{1-e^2} \frac{\partial \mathcal{R}}{\partial h} - \frac{k}{\mu a^2 \nu} \frac{\sqrt{1-e^2}}{1 + \sqrt{1-e^2}} \frac{\partial \mathcal{R}}{\partial \epsilon}, \quad (2.15)$$

which do not diverge even for  $e = 0$  (e.g. [Moulton 1914](#); [Danby 1988](#); [Murray & Dermott 2000](#)).

We have two sets of the Lagrange planetary equations corresponding to the inner and outer orbits. Unlike a conventional analysis for secular evolution, we do not use the orbit-averaged disturbing function. This is because we are interested in the modulation due to the inner binary whose orbital period is shorter than that of the outer orbit.

## 2.2 Perturbation approach to the Lagrange planetary equations for coplanar near-circular orbits

Next we adopt the hierarchical ( $\alpha \ll 1$ ) and near-circular ( $e_{\text{in}} \approx 0$ ,  $e_{\text{out}} \approx 0$ ) conditions, and approximate the disturbing function, neglecting the higher-order terms than  $\mathcal{O}(e^2)$  and  $\mathcal{O}(\alpha^3)$ . Under this approximation, the disturbing function reduces to the quadrupole moment part of the potential:

$$\begin{aligned} \mathcal{R} \approx & \frac{G\mu_1 m_3}{a_{\text{out}}} \alpha^2 \left\{ \frac{1}{4} + \frac{3}{4} \cos(2\lambda_{\text{in}} - 2\lambda_{\text{out}}) + \frac{3}{4} (k_{\text{out}} \cos \lambda_{\text{out}} + h_{\text{out}} \sin \lambda_{\text{out}}) \right. \\ & - \frac{3}{8} [k_{\text{out}} \cos(2\lambda_{\text{in}} - \lambda_{\text{out}}) + h_{\text{out}} \sin(2\lambda_{\text{in}} - \lambda_{\text{out}})] + \frac{21}{8} [k_{\text{out}} \cos(2\lambda_{\text{in}} - 3\lambda_{\text{out}}) - h_{\text{out}} \sin(2\lambda_{\text{in}} - 3\lambda_{\text{out}})] \\ & \left. - \frac{1}{2} (k_{\text{in}} \cos \lambda_{\text{in}} + h_{\text{in}} \sin \lambda_{\text{in}}) - \frac{9}{4} [k_{\text{in}} \cos(\lambda_{\text{in}} - 2\lambda_{\text{out}}) - h_{\text{in}} \sin(\lambda_{\text{in}} - 2\lambda_{\text{out}})] + \frac{3}{4} [k_{\text{in}} \cos(3\lambda_{\text{in}} - 2\lambda_{\text{out}}) + h_{\text{in}} \sin(3\lambda_{\text{in}} - 2\lambda_{\text{out}})] \right\}, \end{aligned} \quad (2.16)$$

where

$$h_{\text{in}} \equiv e_{\text{in}} \sin \varpi_{\text{in}}, \quad k_{\text{in}} \equiv e_{\text{in}} \cos \varpi_{\text{in}}, \quad h_{\text{out}} \equiv e_{\text{out}} \sin \varpi_{\text{out}}, \quad k_{\text{out}} \equiv e_{\text{out}} \cos \varpi_{\text{out}}. \quad (2.17)$$

Finally, we insert equation (2.16) into the Lagrange planetary equations for the outer orbital elements, and obtain the following perturbation equations:

$$\dot{a}_{\text{out}} \approx 3 \frac{m_1 m_2}{m_{12}^2} v_{\text{out}} a_{\text{out}} \alpha^2 \sin(2\lambda_{\text{in}} - 2\lambda_{\text{out}}), \quad (2.18)$$

$$\dot{\epsilon}_{\text{out}} \approx \frac{3}{2} \frac{m_1 m_2}{m_{12}^2} v_{\text{out}} \alpha^2 [1 + 3 \cos(2\lambda_{\text{in}} - 2\lambda_{\text{out}})], \quad (2.19)$$

$$\dot{h}_{\text{out}} \approx \frac{m_1 m_2}{m_{12}^2} v_{\text{out}} \alpha^2 \left[ \frac{3}{4} \cos \lambda_{\text{out}} - \frac{3}{8} \cos(2\lambda_{\text{in}} - \lambda_{\text{out}}) + \frac{21}{8} \cos(2\lambda_{\text{in}} - 3\lambda_{\text{out}}) \right], \quad (2.20)$$

$$\dot{k}_{\text{out}} \approx -\frac{m_1 m_2}{m_{12}^2} v_{\text{out}} \alpha^2 \left[ \frac{3}{4} \sin \lambda_{\text{out}} - \frac{3}{8} \sin(2\lambda_{\text{in}} - \lambda_{\text{out}}) - \frac{21}{8} \sin(2\lambda_{\text{in}} - 3\lambda_{\text{out}}) \right]. \quad (2.21)$$

## 3 ANALYTIC SOLUTIONS TO THE PERTURBATION EQUATIONS

### 3.1 Leading-order solutions

While it is not possible to find exact solutions for equations (2.18)–(2.21), we can solve them iteratively. In practice, we perform the iteration just once, and write down the approximate analytical solutions as follows:

$$\frac{a_{\text{out}}}{a_{\text{out}}^{(i)}} \approx 1 - \frac{3}{2} \frac{m_1 m_2}{m_{12}^2} \frac{v_{\text{out}}^{(i)}}{v_{\text{in}}^{(i)} - v_{\text{out}}^{(i)}} \alpha^2 C_0 [2(v_{\text{in}}^{(i)} - v_{\text{out}}^{(i)})t + 2(\epsilon_{\text{in}}^{(i)} - \epsilon_{\text{out}}^{(i)})], \quad (3.1)$$

$$\epsilon_{\text{out}} \approx \epsilon_{\text{out}}^{(i)} + \frac{3}{2} \frac{m_1 m_2}{m_{12}^2} \alpha^2 v_{\text{out}}^{(i)} t + \frac{9}{4} \frac{m_1 m_2}{m_{12}^2} \frac{v_{\text{out}}^{(i)}}{v_{\text{in}}^{(i)} - v_{\text{out}}^{(i)}} \alpha^2 S_0 [2(v_{\text{in}}^{(i)} - v_{\text{out}}^{(i)})t + 2(\epsilon_{\text{in}}^{(i)} - \epsilon_{\text{out}}^{(i)})], \quad (3.2)$$

$$\begin{aligned} h_{\text{out}} \approx & h_{\text{out}}^{(i)} + \frac{m_1 m_2}{m_{12}^2} \alpha^2 \left[ \frac{3}{4} S_0 [v_{\text{out}}^{(i)} t + \epsilon_{\text{out}}^{(i)}] - \frac{3}{8} \frac{v_{\text{out}}^{(i)}}{2v_{\text{in}}^{(i)} - v_{\text{out}}^{(i)}} S_0 [(2v_{\text{in}}^{(i)} - v_{\text{out}}^{(i)})t + (2\epsilon_{\text{in}}^{(i)} - \epsilon_{\text{out}}^{(i)})] \right. \\ & \left. + \frac{21}{8} \frac{v_{\text{out}}^{(i)}}{2v_{\text{in}}^{(i)} - 3v_{\text{out}}^{(i)}} S_0 [(2v_{\text{in}}^{(i)} - 3v_{\text{out}}^{(i)})t + (2\epsilon_{\text{in}}^{(i)} - 3\epsilon_{\text{out}}^{(i)})] \right], \end{aligned} \quad (3.3)$$

$$\begin{aligned} k_{\text{out}}(t) \approx & k_{\text{out}}^{(i)} + \frac{m_1 m_2}{m_{12}^2} \alpha^2 \left[ \frac{3}{4} C_0 [v_{\text{out}}^{(i)} t + \epsilon_{\text{out}}^{(i)}] - \frac{3}{8} \frac{v_{\text{out}}^{(i)}}{2v_{\text{in}}^{(i)} - v_{\text{out}}^{(i)}} C_0 [(2v_{\text{in}}^{(i)} - v_{\text{out}}^{(i)})t + (2\epsilon_{\text{in}}^{(i)} - \epsilon_{\text{out}}^{(i)})] \right. \\ & \left. - \frac{21}{8} \frac{v_{\text{out}}^{(i)}}{2v_{\text{in}}^{(i)} - 3v_{\text{out}}^{(i)}} C_0 [(2v_{\text{in}}^{(i)} - 3v_{\text{out}}^{(i)})t + (2\epsilon_{\text{in}}^{(i)} - 3\epsilon_{\text{out}}^{(i)})] \right], \end{aligned} \quad (3.4)$$

where

$$C_0[g(t)] \equiv \cos[g(t)] - \cos[g(t=0)], \quad S_0[g(t)] \equiv \sin[g(t)] - \sin[g(t=0)]. \quad (3.5)$$

Note that  $g(t)$  is an arbitrary function of time. In the above expressions and in what follows, the superscript (i) denotes the values for those variables evaluated at the arbitrarily chosen initial epoch ( $t = 0$ ). We also stress that  $\alpha$  denotes  $a_{\text{in}}^{(i)}/a_{\text{out}}^{(i)}$  hereafter, instead of  $a_{\text{in}}(t)/a_{\text{out}}(t)$ , just to simplify the notation.

Equations (3.1) – (3.4) show that the modulation terms of orbital elements are dominated by 2:2, 2:1 and 2:3 harmonics that corresponds to the quadrupole perturbation by the inner binary.

### 3.2 Perturbative analytic expressions for radial velocity

The next task is to derive observable quantities from the solution obtained in §3.1, including variations of the position and radial velocity of the outer body. We focus on the radial velocity (RV) of the outer star, assuming that the precise RV follow-up is performed to search for a possible unseen inner binary.

For an edge-on system, the RV of the outer star in the barycentric coordinate system is

$$V_{\text{RV}}(t) = \frac{m_{12}}{m_{123}} \frac{v_{\text{out}}(t)a_{\text{out}}(t)}{\sqrt{1-e_{\text{out}}(t)^2}} [e_{\text{out}}(t) \cos \omega_{\text{out}}(t) + \cos[f_{\text{out}}(t) + \omega_{\text{out}}(t)]]. \quad (3.6)$$

If  $\sin i_{\text{orb}} \neq 1.0$ , the observable RV is simply obtained by multiplying  $\sin i_{\text{orb}}$  in equation (3.6). In reality, the RV is written in terms of the argument of pericentre  $\omega$ , instead of  $\varpi \equiv \omega + \Omega$  with  $\Omega$  being the longitude of the ascending node. Because we focus on a coplanar system in the present paper, however, we set  $\Omega = 0$  and thus  $\omega = \varpi$  without loss of generality.

Neglecting those terms higher than  $O(e^2)$ , we obtain

$$V_{\text{RV}}(t) \approx \frac{m_{12}}{m_{123}} \{v_{\text{out}}(t)a_{\text{out}}(t) \cos[\lambda_{\text{out}}(t)] + v_{\text{out}}(t)a_{\text{out}}(t)k_{\text{out}}(t) \cos[2\lambda_{\text{out}}(t)] + v_{\text{out}}(t)a_{\text{out}}(t)h_{\text{out}}(t) \sin[2\lambda_{\text{out}}(t)]\}, \quad (3.7)$$

where  $\lambda_{\text{out}}(t)$  is computed through

$$\lambda_{\text{out}}(t) = \int_0^t v_{\text{out}}(t') dt' + \epsilon_{\text{out}}(t). \quad (3.8)$$

Equation (3.7) is further approximated by using the results in §3.1 and  $v_{\text{out}}^{(i)}/v_{\text{in}}^{(i)} \approx (m_{12}/m_{123})^{-1/2} \alpha^{3/2}$ , and by neglecting terms higher than  $O(\alpha^5)$  and  $O(e\alpha^2)$ . Then, we introduce the 3 following terms according to their physical origins:

$$V_{\text{RV}} \approx V_{\text{Kep}} + V_{\text{ecc}} + V_{\text{binary}}. \quad (3.9)$$

The above  $V_{\text{Kep}}$ ,  $V_{\text{ecc}}$  and  $V_{\text{binary}}$  are further divided into several terms according to the frequency and order:

$$V_{\text{Kep}} \equiv V_{\text{Kep}1} + V_{\text{Kep}2} + V_{\text{Kep}3}, \quad (3.10)$$

$$V_{\text{ecc}} \equiv V_{\text{ecc}1} + V_{\text{ecc}2} + V_{\text{ecc}3}, \quad (3.11)$$

$$V_{\text{binary}} \equiv V_{\text{binary}1} + V_{\text{binary}2} + V_{\text{binary}3} + V_{\text{binary}4}. \quad (3.12)$$

The explicit expressions for the frequencies and amplitudes of these terms are listed in Table 3.

Equation (3.10) basically corresponds to the Kepler motion of the outer body, but their orbital frequencies deviate very slightly from  $\nu = \nu_{\text{out}}^{(i)}$  due to the presence of the inner binary. Since the frequency difference  $\Delta\nu_{\text{out}}$  is small, the three frequencies may be practically indistinguishable from  $\nu_{\text{out}}^{(i)}$ .

Equation (3.11) with  $\nu = 2\nu_{\text{out}}^{(i)}$  comes from the second and third terms in equation (3.7), representing the first-order expansion of the true anomaly  $f$  in terms of  $e$  and  $\lambda$ . Since this term shows up always for non-circular orbits, it is not directly related to the presence of the inner binary.

Equation (3.12) with  $\nu = 2\nu_{\text{in}}^{(i)}$  represents the velocity modulation due to the quadrupole moment of the inner binary, keeping information of the inner binary. Therefore, we use the word “signals” referring to  $V_{\text{binary}}$ . We can see from Table 3 that  $V_{\text{binary}}$  consists of four modes with practically  $2\nu_{\text{in}} - \nu_{\text{out}}$  and  $2\nu_{\text{in}} - 3\nu_{\text{out}}$  frequencies. Combining the four terms of  $V_{\text{binary}1}$  to  $V_{\text{binary}4}$ , we can see its structure effectively:

$$V_{\text{binary}} \equiv V_{\text{binary}1} + V_{\text{binary}2} + V_{\text{binary}3} + V_{\text{binary}4} \approx \frac{3}{8} K_{\text{BBH}} \cos[2(\nu_{\text{in}}^{(i)} - \nu_{\text{out}}^{(i)})t + 2(\epsilon_{\text{in}}^{(i)} - \epsilon_{\text{out}}^{(i)})] \cos[\nu_{\text{out}}^{(i)}t + \epsilon_{\text{out}}^{(i)}] - \frac{9}{8} K_{\text{BBH}} \cos[(2\nu_{\text{in}}^{(i)} - \nu_{\text{out}}^{(i)})t + 2\epsilon_{\text{in}}^{(i)} - \epsilon_{\text{out}}^{(i)}], \quad (3.13)$$

where

$$K_{\text{BBH}} \equiv \frac{m_{12}}{m_{123}} \sqrt{\frac{Gm_{123}}{a_{\text{out}}^{(i)}}} \left( \sqrt{\frac{m_1}{m_2}} + \sqrt{\frac{m_2}{m_1}} \right)^{-2} \left( \frac{m_{12}}{m_{123}} \right)^{-\frac{1}{2}} \alpha^{\frac{7}{2}}. \quad (3.14)$$

The first term in equation (3.13) is a cosine wave of  $2(\nu_{\text{in}} - \nu_{\text{out}})$  frequency with the beating effect of  $\nu_{\text{out}}/2$  frequency. The second term is a cosine wave of  $2\nu_{\text{in}} - \nu_{\text{out}}$  frequency. Therefore, equation (3.13) indicates that the  $V_{\text{binary}}$  are dominated by 2 : 2 and 2 : 1 harmonics for short-term signals but its amplitude shows gradual changes with time through the beating effect.

We may estimate the values of  $\nu_{\text{in}}^{(i)}$  and  $K_{\text{BBH}}$  from those signals. Since the parameters characterizing the outer orbit,  $V_{\text{RV},0}$ ,  $a_{\text{out}}$  and  $m_3$  should be known from  $V_{\text{Kep}}$  and spectroscopic analysis of the outer star, we can obtain  $m_1$ ,  $m_2$  and  $a_{\text{in}}$  separately from  $V_{\text{binary}}$ , or constrain those parameters even from the upper limits on  $V_{\text{binary}}$ .

While  $V_{\text{binary}}$  is obtained precisely from the perturbation expansion, it can be also derived more qualitatively as follows. Consider a simplified model illustrated in Figure 2. If we neglect the motion of the outer body ( $m_3$ ) during one orbital period

symbol	expression
$\alpha$	$a_{\text{in}}^{(i)}/a_{\text{out}}^{(i)}$
$\beta$	$m_{12}/m_{123}$
$\gamma$	$\sqrt{m_2/m_1} + \sqrt{m_1/m_2}$
$V_{\text{RV},0}$	$\beta v_{\text{out}}^{(i)} a_{\text{out}}^{(i)}$
$\Delta v_{\text{out}}/v_{\text{out}}^{(i)}$	$\frac{3}{2}\alpha^2\gamma^{-2}\left[1 - \frac{3}{2}\beta^{-\frac{1}{2}}\alpha^{\frac{3}{2}}\cos[2(\epsilon_{\text{in}}^{(i)} - \epsilon_{\text{out}}^{(i)})]\right]$
$p(t)$	$\frac{9}{4}\alpha^{\frac{7}{2}}\beta^{-\frac{1}{2}}\gamma^{-2}S_0[2(v_{\text{in}}^{(i)} - v_{\text{out}}^{(i)})t + 2(\epsilon_{\text{in}}^{(i)} - \epsilon_{\text{out}}^{(i)})]$
$K_{\text{BBH}}$	$V_{\text{RV},0}\alpha^{\frac{7}{2}}\beta^{-\frac{1}{2}}\gamma^{-2}$

**Table 2.** The variables used to describe the explicit expressions of each RV modes.

symbol	$\nu$ (frequency)	expression
$V_{\text{Kep1}}$	$v_{\text{out}}^{(i)} + \Delta v_{\text{out}}$	$V_{\text{RV},0} \cos(\nu t + p(t) + \epsilon_{\text{out}}^{(i)})$
$V_{\text{Kep2}}$	$v_{\text{out}}^{(i)} + 2\Delta v_{\text{out}}$	$\frac{3}{4}V_{\text{RV},0}\alpha^2\gamma^{-2} \cos(\nu t + 2p(t) + \epsilon_{\text{out}}^{(i)})$
$V_{\text{Kep3}}$	$v_{\text{out}}^{(i)} + \Delta v_{\text{out}}$	$-\frac{3}{8}K_{\text{BBH}} \left[ \cos(\nu t + p(t) + 2\epsilon_{\text{in}}^{(i)} - \epsilon_{\text{out}}^{(i)}) + \cos(\nu t + p(t) - 2\epsilon_{\text{in}}^{(i)} + 3\epsilon_{\text{out}}^{(i)}) \right]$
$V_{\text{ecc1}}$	$2(v_{\text{out}}^{(i)} + \Delta v_{\text{out}})$	$h_{\text{out}}^{(i)}V_{\text{RV},0} \sin(\nu t + 2p(t) + 2\epsilon_{\text{out}}^{(i)}) + k_{\text{out}}^{(i)}V_{\text{RV},0} \cos(\nu t + 2p(t) + 2\epsilon_{\text{out}}^{(i)})$
$V_{\text{ecc2}}$	$2(v_{\text{out}}^{(i)} + \Delta v_{\text{out}})$	$-\frac{3}{4}V_{\text{RV},0}\alpha^2\gamma^{-2} \cos(\nu t + 2p(t) + \epsilon_{\text{out}}^{(i)})$
$V_{\text{ecc3}}$	$2(v_{\text{out}}^{(i)} + \Delta v_{\text{out}})$	$\frac{3}{16}K_{\text{BBH}} \left[ 7\cos(\nu t + 2p(t) + 2\epsilon_{\text{in}}^{(i)} - \epsilon_{\text{out}}^{(i)}) + \cos(\nu t + 2p(t) - 2\epsilon_{\text{in}}^{(i)} + 3\epsilon_{\text{out}}^{(i)}) \right]$
$V_{\text{binary1}}$	$2v_{\text{in}}^{(i)} - v_{\text{out}}^{(i)} + 2\Delta v_{\text{out}}$	$-\frac{21}{16}K_{\text{BBH}} \cos(\nu t + 2p(t) + 2\epsilon_{\text{in}}^{(i)} - \epsilon_{\text{out}}^{(i)})$
$V_{\text{binary2}}$	$2v_{\text{in}}^{(i)} - v_{\text{out}}^{(i)} + \Delta v_{\text{out}}$	$\frac{3}{8}K_{\text{BBH}} \cos(\nu t + p(t) + 2\epsilon_{\text{in}}^{(i)} - \epsilon_{\text{out}}^{(i)})$
$V_{\text{binary3}}$	$2v_{\text{in}}^{(i)} - 3v_{\text{out}}^{(i)} - \Delta v_{\text{out}}$	$\frac{3}{8}K_{\text{BBH}} \cos(\nu t - p(t) + 2\epsilon_{\text{in}}^{(i)} - 3\epsilon_{\text{out}}^{(i)})$
$V_{\text{binary4}}$	$2v_{\text{in}}^{(i)} - 3v_{\text{out}}^{(i)} - 2\Delta v_{\text{out}}$	$-\frac{3}{16}K_{\text{BBH}} \cos(\nu t - 2p(t) + 2\epsilon_{\text{in}}^{(i)} - 3\epsilon_{\text{out}}^{(i)})$
$V_{\text{Kep}}$	$\approx v_{\text{out}}^{(i)}$	$V_{\text{Kep1}} + V_{\text{Kep2}} + V_{\text{Kep3}} \approx V_{\text{Kep1}}$
$V_{\text{ecc}}$	$\approx 2v_{\text{out}}^{(i)}$	$V_{\text{ecc1}} + V_{\text{ecc2}} + V_{\text{ecc3}} \approx V_{\text{ecc1}} + V_{\text{ecc2}}$
$V_{\text{binary}}$	$\approx 2v_{\text{in}}^{(i)}$	$V_{\text{binary1}} + V_{\text{binary2}} + V_{\text{binary3}} + V_{\text{binary4}}$

**Table 3.** Ten terms for the radial velocity of the outer body from the approximate analytic solutions. The tiny correction to orbital frequency  $\Delta v_{\text{out}}$  shows up due to the secular growth of  $\epsilon$ . The  $p(t)$  and  $\Delta v_{\text{out}}$  are very small since they are proportional to  $\mathcal{O}(\alpha^{7/2})$  and  $\mathcal{O}(\alpha^2)$  respectively compared with  $v_{\text{in}}$  and  $v_{\text{out}}$ . Therefore, we can regard them as zero practically. However, we keep them here for the later numerical comparisons.

of the inner binary  $P_{\text{in}}(\ll P_{\text{out}})$ , the force  $\mathcal{F}$  acting on  $m_3$  toward  $Y$  direction in Figure 2 is given by

$$\begin{aligned}
 \mathcal{F} = & \frac{Gm_1m_3 \left( -a_{\text{out}} - \frac{m_2}{m_{12}}a_{\text{in}} \cos(v_{\text{in}}t) \right)}{\left[ \left( \frac{m_2}{m_{12}}a_{\text{in}} \sin(v_{\text{in}}t) \right)^2 + \left( -a_{\text{out}} - \frac{m_2}{m_{12}}a_{\text{in}} \cos(v_{\text{in}}t) \right)^2 \right]^{3/2}} + \frac{Gm_2m_3 \left( -a_{\text{out}} + \frac{m_1}{m_{12}}a_{\text{in}} \cos(v_{\text{in}}t) \right)}{\left[ \left( -\frac{m_1}{m_{12}}a_{\text{in}} \sin(v_{\text{in}}t) \right)^2 + \left( -a_{\text{out}} + \frac{m_1}{m_{12}}a_{\text{in}} \cos(v_{\text{in}}t) \right)^2 \right]^{3/2}} \\
 \approx & -\frac{Gm_{12}m_3}{a_{\text{out}}^2} - \frac{3Gm_1m_2m_3}{4a_{\text{out}}^2m_{12}} - \frac{9Gm_1m_2m_3}{4a_{\text{out}}^2m_{12}} \cos(2v_{\text{in}}t).
 \end{aligned} \tag{3.15}$$

The first term in the right-hand-side corresponds to the Keplerian motion of  $m_3$ , the second term induce a constant tiny change on the Keplerian motion, and the third term represents the periodic modulation due to the inner binary. Therefore,



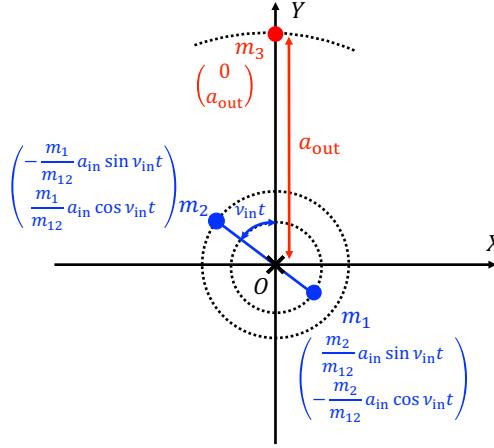


**Figure 2.** A simplified model to derive  $V_{\text{binary}}$  qualitatively. The cross denotes the center of mass for the inner binary.

the amplitude of the velocity modulation  $\delta V$  is roughly estimated as

$$\delta V \approx \int_0^t -\frac{9Gm_1m_2}{4a_{\text{out}}^2m_{12}} \cos(2v_{\text{in}}t') dt' \approx -\frac{9}{8} K_{\text{BBH}} \sin(2v_{\text{in}}t). \quad (3.16)$$

This expression qualitatively reproduces the overall amplitude and frequency of  $V_{\text{binary}}$ .

On the basis of the approximate solutions that we have obtained, we propose a methodology to search for an inner binary signal from the RV of the outer body, which is schematically illustrated in Figures 3 and 4. We focus on a binary candidate of a star ( $m_3$ ) and an unseen object ( $m_{12} = m_1 + m_2$ ), presumably a BBH of  $m_1$  and  $m_2$ . The RV of the outer star is dominated by its Kepler motion,  $V_{\text{Kep}}$ , with the orbital period of  $P_{\text{out}}$  (Fig. 3). In order to see whether the unseen object is an inner binary system, the shorter-cadence RV follow-up with higher precision is performed for a short duration. If it is indeed the case, the smaller amplitude modulation with the shorter period  $P_{\text{in}}/2$  should show up in the RV signal after removing  $V_{\text{Kep}}$  and  $V_{\text{ecc}}$  (Fig. 4).

In those figures, we consider a system of  $\epsilon_{\text{in}}^{(i)} = \pi/6$ ,  $\epsilon_{\text{out}}^{(i)} = 2\pi/3$ , and  $\varpi_{\text{in}}^{(i)} = \varpi_{\text{out}}^{(i)} = 0$ , and the other initial parameters are indicated there. The RV is computed from our approximate analytic solution that is labeled by the subscript *app*. The validity of the approximated solution is examined against the numerical simulation in Appendix A.

#### 4 APPLICATION TO A BINARY SYSTEM 2M05215658+4359220

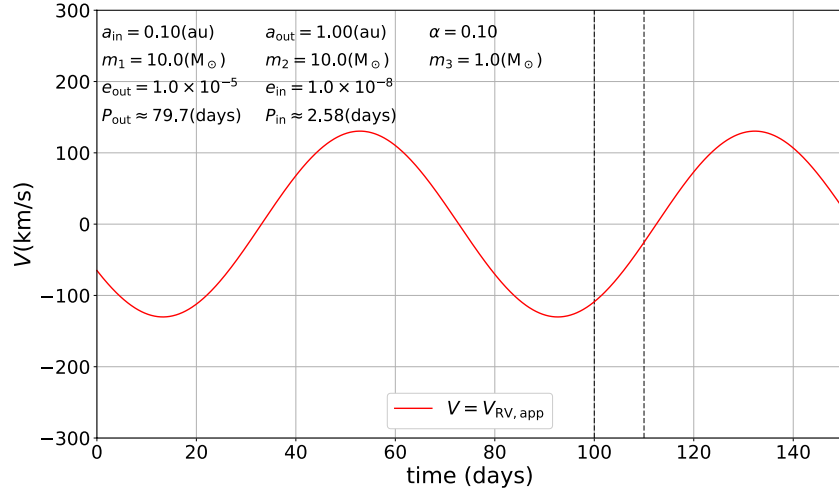
Thompson et al. (2018) reported the discovery of a binary system 2M05215658+4359220 that consists of a red giant and an unseen massive object. They first searched for systems exhibiting anomalously large radial accelerations from the Apache Point Observatory Galactic Evolution Experiment (APOGEE) radial velocity data, and selected 200 candidates of such binaries. After checking the photometric variations from the All-Sky Automated Survey for Supernovae (ASAS-SN) data, they identified 2M05215658+4359220 as the most likely binary candidate. Subsequently, they performed the radial velocity follow-up observation with the Tillinghast Reflector Echelle Spectrograph (TRES) on the 1.5 m telescope at the Fred Lawrence Whipple Observatory (FLWO). They obtained 11 spectra with the precision of about  $0.1 \text{ km s}^{-1}$  over several months in 2017 and 2018.

Interestingly, the orbital period of the system turned out to be very close to that of the photometric variation of the star, indicating the tidal synchronization. Therefore they assume that the inclination of the rotation axis of the outer red giant  $i_{\text{rot}}$  is equal to its orbital inclination  $i_{\text{orb}}$ :  $i \equiv i_{\text{rot}} = i_{\text{orb}}$ . This enabled them to estimate the best-fit parameters of the system (Table 4) from the RV data and the spectroscopic analysis of the red giant.

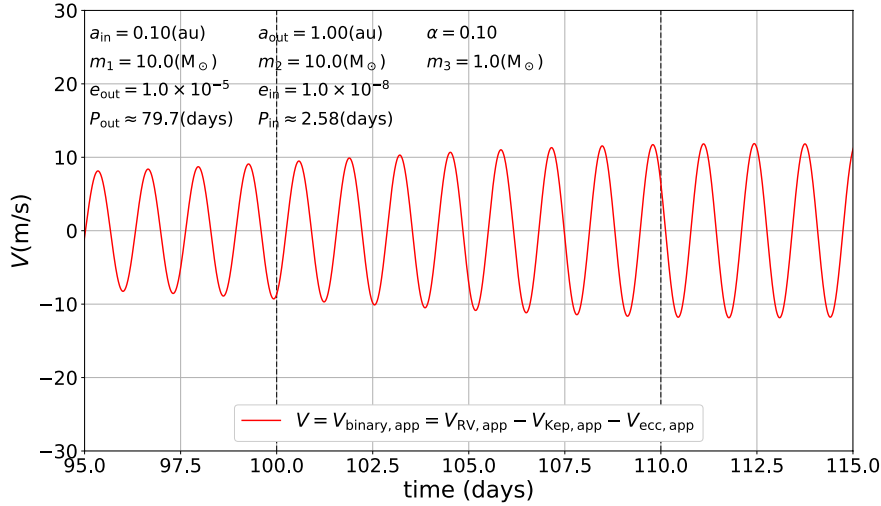
Thompson et al. (2018) estimated the mass of the unseen companion to be  $m_{\text{CO}} = 3.2_{-0.4}^{+1.1} M_{\odot}$ . Since the value may exceed the conventionally accepted range of the maximum mass of the neutron star, it could be a single black hole as well, or even a binary neutron star/black hole. We assume that the inner binary is near-circular and coplanar with the outer orbit, and set  $m_{\text{giant}} = m_3$  and  $m_{\text{CO}} = m_1 + m_2$ ; see Table 4. Then we apply our approximate solutions so as to constrain the viable parameters for the possible inner binary.

Figure 5 plots a color contour map of the amplitude of  $K_{\text{BBH}}$  as a function of the mass ratio  $m_2/m_1$  and the orbital period  $P_{\text{in}}$  of the possible inner binary for the 2M05215658+4359220 system. We compute the value of  $K_{\text{BBH}}$  from equation (3.14) using the parameters listed in Table 4. The color is coded according to the value of  $K_{\text{BBH}}$  that labels the contour curves. While Figure 5 assumes the edge-on orbit ( $i_{\text{orb}} = \pi/2$ ), the contour is also valid for the inclined case if the value of  $K_{\text{BBH}}$  is re-interpreted as  $V_{\text{binary}} \sin i_{\text{orb}}$ .





**Figure 3.** The total RV of outer star orbiting around an inner binary calculated from the approximation formula. The initial parameters are shown in the figure. The time interval between  $t = 100$  day and  $t = 110$  day is marked as the inside of two dashed lines.



**Figure 4.** The  $V_{\text{binary}}$  from the approximation formula. The two dashed lines denote  $t = 100$  day and  $t = 110$  day corresponding to the time interval in Figure 3. The gradual change of amplitude reflects the beating effect (see equation (3.13) and Figure A5).

parameter	value	meaning
$P_{\text{out}}$	$83.205 \pm 0.064$ days	orbital period
$m_{\text{co}}$	$3.2^{+1.1}_{-0.4} M_{\odot}$	mass of an unseen companion
$m_{\text{giant}}$	$3.0^{+0.6}_{-0.5} M_{\odot}$	mass of a red giant
$e_{\text{out}}$	$0.0048 \pm 0.0026$	eccentricity
$\varpi_{\text{out}}$	$197.13 \pm 32.07$ deg	longitude of pericentre
$\sin i$	$0.97^{+0.02}_{-0.14}$	inclination of the orbital plane
$R_{\text{giant}}$	$23.8^{+3.9}_{-0.6} R_{\odot}$	radius of a red giant

**Table 4.** A list of parameters for the binary system 2M05215658+4359220 (Thompson et al. 2018)

The axis on the right indicates the semi-major axis ratio  $\alpha$  corresponding to the orbital period  $P_{\text{in}}$  of the left axis. Because our approximate solutions are derived for  $\alpha \ll 1$ , their accuracy is degraded towards the upper part of Figure 5. We will discuss the validity of the result later by comparing with the numerical simulation. Indeed the three-body system becomes dynamically unstable if it satisfies

$$\alpha > \left( \frac{a_{\text{in}}}{a_{\text{out}}} \right)_{\text{crit}} \equiv \frac{1 - e_{\text{out}}}{2.8} \left( \frac{(1 + m_3/(m_1 + m_2))(1 + e_{\text{out}})}{\sqrt{1 - e_{\text{out}}}} \right)^{-\frac{2}{5}} \approx 0.272 \quad (4.1)$$

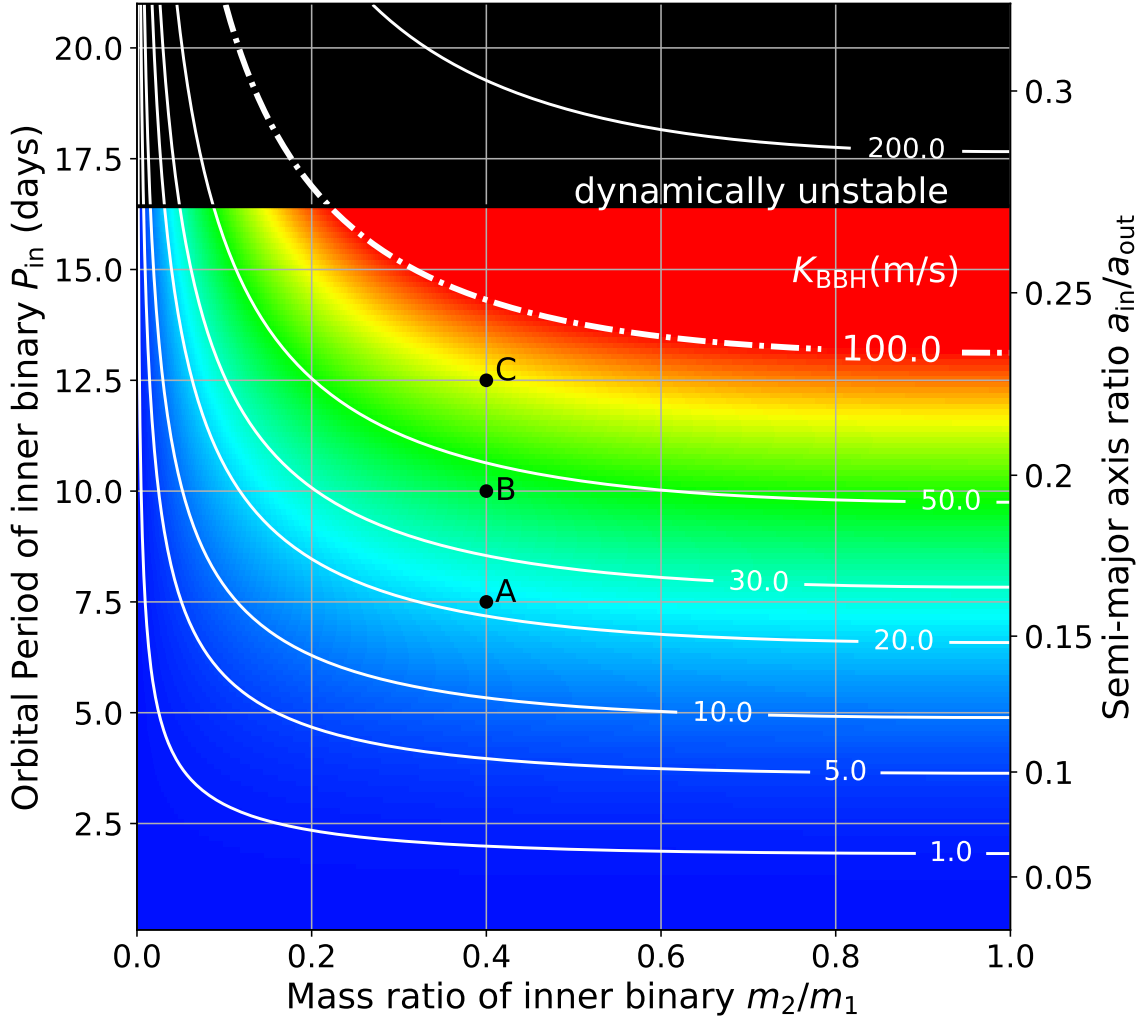


**Figure 5.** The estimated RV modulations  $K_{\text{BBH}}$  due to the inner binary for 2M05215658+4359220 (Eq. (3.14)). Each contour curve is labeled by the value of  $K_{\text{BBH}}$  in units of m/s. The black region specifies the dynamically unstable region calculated by equation (4.1).

(Mardling & Aarseth 2001). Thus our perturbation result completely breaks down there as indicated by the black area in Figure 5.

Even the current RV data are consistent with a simple Keplerian orbit of the outer red giant within the observational error of  $\sim 100$  m/s (Thompson et al. 2018), while it is not so precise. In turn, even the current data may be interpreted to exclude the region beyond  $V_{\text{binary}} = 100/\sin i_{\text{orb}} \approx 100$  in Figure 5. If the precision of the RV measurement could be improved with an intensive follow-up over a few months, the resulting constraint would become stronger, or even a signature of the presence of the unseen inner binary might be detected.

As we mentioned earlier, however, the reliability of our perturbation formulae is not guaranteed when  $\alpha > 0.1$ , for instance. Thus we attempt to check the validity of the constraints against numerical simulations. Specifically, we consider three cases, black circles labeled A, B, and C in Figure 5, whose parameters are summarized in Tables 5 and 6. The three cases adopt the same mass ratio  $m_2/m_1 (= 0.4)$ , but different orbital periods of the inner binary  $P_{\text{in}}$ . Since  $\alpha$  monotonically increases with  $P_{\text{in}}$ , the accuracy of the approximate formula would be degraded for larger  $P_{\text{in}}$ .

Figure 6 (a) - (c) compare  $V_{\text{binary}}$  computed with the perturbation formulae (red) and numerical simulations (blue) for the three cases. While these plots show that  $V_{\text{binary}}$  computed from simulations are affected by the longer-term modulation with a period of  $P_{\text{out}}$ , the amplitude of the RV modulation due to the inner binary is generally *underestimated* by a factor of few relative to the numerical result. Furthermore,  $V_{\text{binary}}$  is very similar to  $K_{\text{BBH}}$  itself, implying that the different phases among  $V_{\text{binary}1}$ ,  $V_{\text{binary}2}$ ,  $V_{\text{binary}3}$ , and  $V_{\text{binary}4}$  do not cancel the overall amplitude of  $V_{\text{binary}}$ . Therefore, the constraints plotted in Figure 5 should be rather regarded as *conservative*, and serve as a useful analytic limit on a possible inner binary. Note that the long-term modulation with  $P_{\text{out}}$  does not affect the conclusion since only the short-term oscillations are important as the signature of inner binary (see Appendix A for detail).

parameter	value
$a_{\text{out}}$	0.685 au
$m_3$	$3.0 M_{\odot}$
$e_{\text{in}}$	$10^{-8}$
$e_{\text{out}}$	0.0048
$f_{\text{in}}$	$\frac{\pi}{6}$
$f_{\text{out}}$	$\frac{2}{3}\pi$
$\varpi_{\text{in}}$	0.0
$\varpi_{\text{out}}$	$\frac{197.13}{180}\pi$

**Table 5.** Initial parameters common for Cases A to C

parameter	value	Case
$a_{\text{in}}$	0.11 au	A
$P_{\text{in}}$	7.5 days	A
$m_2/m_1$	0.4	A
$(m_1, m_2) M_{\odot}$	(2.29, 0.91)	A
$a_{\text{in}}$	0.13 au	B
$P_{\text{in}}$	10.0 days	B
$m_2/m_1$	0.4	B
$(m_1, m_2) M_{\odot}$	(2.29, 0.91)	B
$a_{\text{in}}$	0.16 au	C
$P_{\text{in}}$	12.5 days	C
$m_2/m_1$	0.4	C
$(m_1, m_2) M_{\odot}$	(2.29, 0.91)	C

**Table 6.** Initial parameters corresponding to Cases A to C

Also independently of the RV amplitude, it is possible to extract its modulation frequency:

$$v_{\text{in}}^{(i)} \equiv \sqrt{\frac{G(m_1 + m_2)}{a_{\text{in}}^{(i)3}}}, \quad (4.2)$$

if the modulation is detected. Then, one can estimate the semi-major axis of the inner binary,  $a_{\text{in}}$ , from  $v_{\text{in}}$  combined with the total mass of the inner bodies  $m_1 + m_2$ .

## 5 DEGENERACY BETWEEN A SYSTEM CONSISTING OF A SINGLE BLACK HOLE AND A PLANET-HOST STAR

So far we have considered the RV modulation of the outer star due to the inner binary with its orbital period of  $P_{\text{in}}$ . The resulting RV signal of a period  $\sim P_{\text{in}}/2$ , however, may be induced by a planet around the star with its orbital period of  $P_{\text{in}}/2$ ; see Figure 7 for schematic illustrations. We find that the two models are intrinsically degenerate in general, either of which is equally interesting. Therefore we discuss the signal due to a planet in this section.

Before considering a general case, we focus on the binary system 2M05215658+4359220 as a specific example. As Figure 5 indicates, the allowed region for the inner binary is  $P_{\text{in}} \lesssim 12.5$  days if we assume that no RV modulation is present within the TRES RV uncertainty of  $\sim 100$  m/s (Thompson et al. 2018). According to Thompson et al. (2018), the outer star is a red giant with the best-fit radius of  $23.8^{+3.9}_{-0.6} R_{\odot} \sim 0.11 \text{ au}$ . This implies that the orbital period of a planet orbiting around this red giant,  $P_{\text{p}}$ , even if exists, should satisfy

$$P_{\text{p}} \approx 7.7 \text{ days} \left( \frac{a_{\text{p}}}{0.11 \text{ au}} \right)^{3/2} > 7.7 \text{ days}, \quad (5.1)$$

where  $a_{\text{p}}$  is the semi-major axis of the planet.

This period would be translated into

$$P_{\text{in}} = 2P_{\text{p}} \approx 15 \text{ days} \left( \frac{a_{\text{p}}}{0.11 \text{ au}} \right)^{3/2} > 15 \text{ days} \quad (5.2)$$

in the inner BBH interpretation. Since the constraint (5.2) is in conflict with the current constraint of  $P_{\text{in}} \lesssim 12.5$  days (Fig. 5), the future possible RV modulation of this system is unlikely to be explained by the planet-star picture.

If the outer star orbiting around an unseen object is a dwarf, unlike in the case of 2M05215658+4359220, a planet around the star induces the RV modulation with very similar amplitude and frequency that we have obtained in section 3. Therefore we consider the degeneracy between the planet-star and inner BBH interpretations, and investigate their parameter correspondence in the rest of this section.

### 5.1 Correspondence between a planet-star and inner binary black-hole interpretations

The RV modulation of the outer body is basically characterized by its amplitude  $K_{\text{mod}}$  and period  $P_{\text{mod}}$ . The former is equal to  $P_{\text{p}}$  and  $P_{\text{in}}/2$  in the planet-star and inner BBH interpretations, respectively.

The RV modulation amplitude induced by an inner BBH (the left panel in Figure 7) is estimated from equation (3.14):

$$K_{\text{BBH}} = (2\pi G)^{1/3} \left( \frac{m_{123}}{m_{12}} \right)^{5/3} P_{\text{out}}^{-1/3} m_{123}^{1/3} \gamma^{-2} \left( \frac{P_{\text{in}}}{P_{\text{out}}} \right)^{7/3}, \quad (5.3)$$

where  $P_{\text{out}}$  is the orbital period of the outer star,  $m_{123} = m_1 + m_2 + m_3$ ,  $m_{12} = m_1 + m_2$ , and  $\gamma \equiv (\sqrt{m_2/m_1} + \sqrt{m_1/m_2})$ .

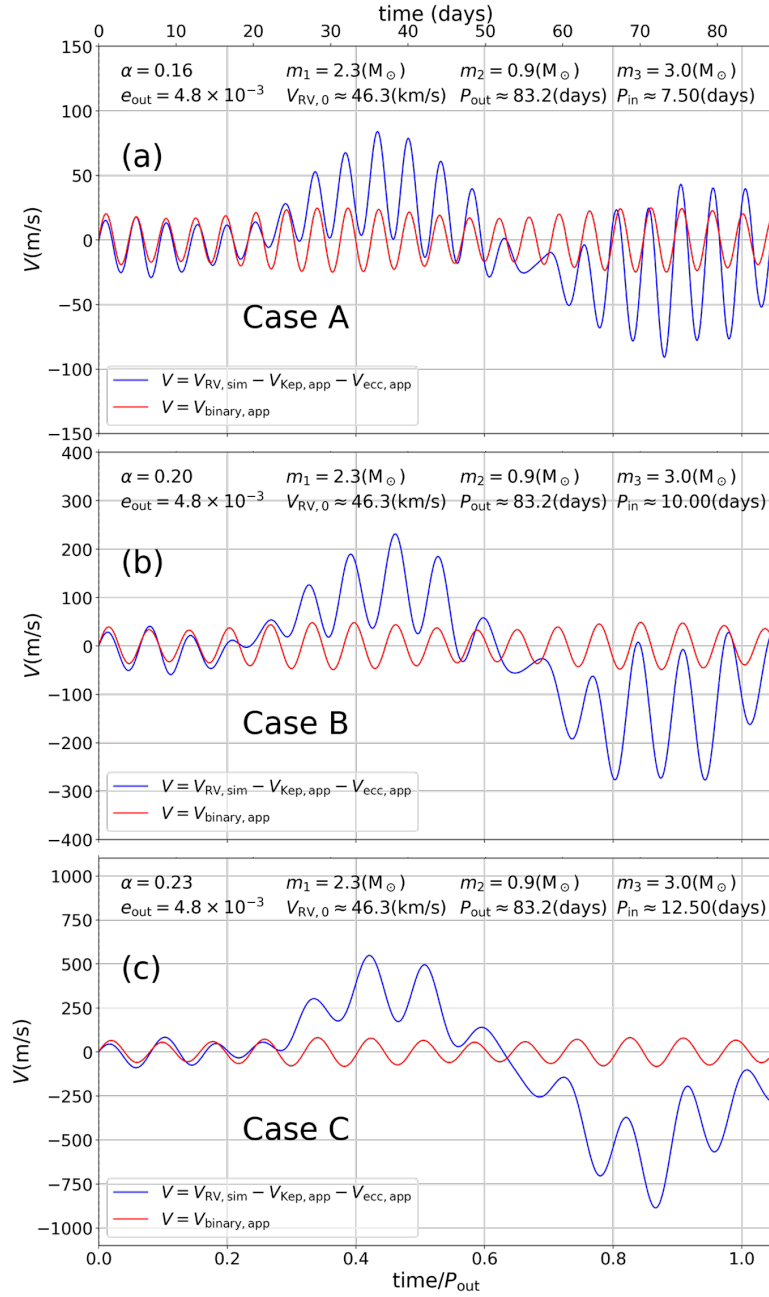


**Figure 6.** Comparison of our approximate formulae against numerical simulation for the system 2M05215658+4359220 assuming the initial parameters shown in Tables 5 and 6: (a) Case A, (b) Case B, and (c) Case C.

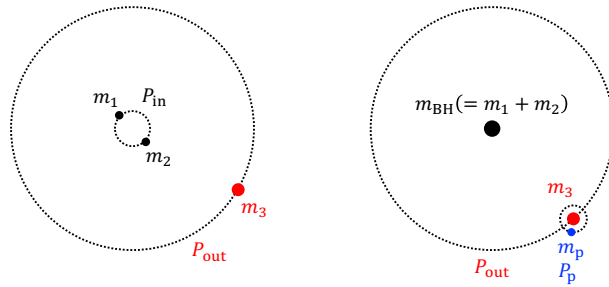


**Figure 7.** Two pictures inducing short-term RV modulations.

The amplitude induced by a planet around the outer star (the right panel in Figure 7), on the other hand, is

$$K_p = (2\pi G)^{1/3} P_p^{-1/3} m_p m_3^{-2/3} = (2\pi G)^{1/3} 2^{1/3} P_{\text{in}}^{-1/3} m_p m_3^{-2/3}, \quad (5.4)$$

where  $m_p$  is the mass of planet, and we assume that  $m_p \ll m_3$  and the orbital period of planet  $P_p$  is identical to  $P_{\text{in}}/2$ .

If we equate  $K_{\text{BBH}}$  and  $K_p$ , the mass of the planet can be written in terms of the parameters in the inner BBH interpretation as

$$m_p = 2^{-1/3} m_3^{2/3} \left( \frac{m_{\text{BH}}}{m_{\text{BH}} + m_3} \right)^{5/3} \gamma^{-2} (m_{\text{BH}} + m_3)^{1/3} \left( \frac{P_{\text{in}}}{P_{\text{out}}} \right)^{8/3}, \quad (5.5)$$

where we define  $m_{\text{BH}} \equiv m_1 + m_2$ . In other words, the inner BBH of  $m_1$  and  $m_2$  with the orbital period of  $P_{\text{in}}$  induces the similar RV modulation of the outer star due to the planet of mass given by equation (5.5), and the orbital period of  $P_p = P_{\text{in}}/2$ . If  $P_p = P_{\text{in}}/2$  and  $K_{\text{BBH}} = K_p$ , both interpretations create similar short-term modulations, therefore we cannot distinguish them without very high precision. In this case, the RV modulation amplitude  $K_{\text{mod}} (= K_{\text{BBH}} = K_p)$  can be written as

$$K_{\text{mod}} = (2\pi G)^{1/3} 2^{7/24} m_p^{7/8} m_3^{-7/12} m_{\text{BH}}^{5/24} (m_{\text{BH}} + m_3)^{-1/6} P_{\text{out}}^{-1/3} \gamma^{-1/4}. \quad (5.6)$$

Equations (5.5) and (5.6) relate the parameters in the two different interpretations. Later, we use them to make plots relating the two interpretations.

## 5.2 Constraints from dynamical instability and gravitational emissions

As we discussed in section 4, the inner BBH interpretation is not viable if the system satisfies

$$\left( \frac{a_{\text{in}}}{a_{\text{out}}} \right) > \frac{1 - e_{\text{out}}}{2.8} \left( \frac{(1 + m_3/(m_1 + m_2))(1 + e_{\text{out}})}{\sqrt{1 - e_{\text{out}}}} \right)^{-2/5} \approx \frac{1}{2.8} \left( \frac{m_{123}}{m_{12}} \right)^{-2/5}, \quad (5.7)$$

where we assume  $e_{\text{out}} \approx 0$ . When we use equation (5.5) and rewrite the above criterion in terms of  $m_p$ , we obtain

$$m_p > 2^{-1/3} 2.8^{-4} m_3^{2/3} \gamma^{-2} (m_{\text{BH}} + m_3)^{1/3} \left( \frac{m_{\text{BH}}}{m_{\text{BH}} + m_3} \right)^{29/15}. \quad (5.8)$$

If the above condition is satisfied, the induced RV modulation should be due to the planet, rather than the the inner BBH because the corresponding system is dynamically unstable.

In the planet-star picture, the planet of mass  $m_p (\ll m_3)$  has a stable orbit around the star of mass  $m_3$  when its semi-major axis  $a_p$  is much less than the Hill radius of the star:

$$a_p < f \left( \frac{m_3}{3m_{\text{BH}}} \right)^{1/3} a_{\text{out}}, \quad (5.9)$$

where  $f = 0.36$  is derived from numerical simulations, and this relation is known to hold for  $\mu \equiv m_{\text{BH}}/(m_{\text{BH}} + m_3) \gtrsim 0.8$  (e.g. Holman & Wiegert 1999; Barnes & O'Brien 2002). Therefore in the planet-star case, equation (5.5) should satisfy

$$m_p < 2^{7/3} 3^{-4/3} f^4 \gamma^{-2} m_3^{2/3} m_{\text{BH}}^{1/3}. \quad (5.10)$$

Incidentally, the time to coalescence  $t_0$  via gravitational wave emissions for an inner circular compact binary consisting of  $m_1$  and  $m_2$  is given by Peters (1964):

$$t_0 = \frac{5}{256} \frac{c^5 a_{\text{in}}^4}{G^3 m_{12}^2 \mu} \approx 1.88 \times 10^{11} \left( \frac{P_{\text{in}}}{\text{day}} \right)^{8/3} \left( \frac{m_{12}}{M_{\odot}} \right)^{-5/3} \text{ yrs}, \quad (5.11)$$

where  $m_{12} \equiv m_1 + m_2$ ,  $\mu \equiv m_1 m_2 / m_{12}$ , and  $a_{\text{in}}$  is the semi-major axis of the inner BBH. Therefore, the inner binary orbit is not affected by the gravitational wave emission unless  $P_{\text{in}} \ll 1$  days.

Figures 8 and 9 show the correspondence between  $m_p$  in the planet-star interpretation and  $m_{\text{BH}} = m_1 + m_2$  in the inner BBH interpretation for  $P_{\text{out}} = 100$  days and 1000 days, respectively. Both figures assume that  $m_2/m_1 = 1$  and  $m_3 = 1 M_{\odot}$ . Given the values of the RV modulation amplitude and period,  $K_{\text{mod}}$  (color-coded) and  $P_{\text{mod}}$  (black contour), the corresponding values of  $m_p$  and  $m_{\text{BH}}$  can be read off from the figures. The dotted area above the blue curve is excluded by the stability of the inner BBH picture. The gray region above the green curve is excluded by the stability of the planet orbiting the star. Most of the range of  $K_{\text{mod}}$  and  $P_{\text{mod}}$  except those exclusion regions indeed permit the two different interpretations as the origin of the RV modulation. In order to break the degeneracy of two interpretations, it would be required to catch up the gradual change of amplitude due to beating effect (see equation 3.13) with very precise observation and analysis.

## 6 SUMMARY

In near future, we expect to detect a number of stars orbiting around invisible objects. A fraction of them may be a triple system consisting of an inner binary black hole and an outer orbiting star. In this paper, we have proposed a methodology to search for a signature of the inner BBH, possibly a progenitor of gravitational wave sources recently detected by *LIGO*, from the precise radial velocity follow-up of the outer star. Although this methodology cannot differentiate any invisible inner binary ( *etc* binary black hole, binary neutron star), the electromagnetic counterpart will give us some information once we identify the inner binary.

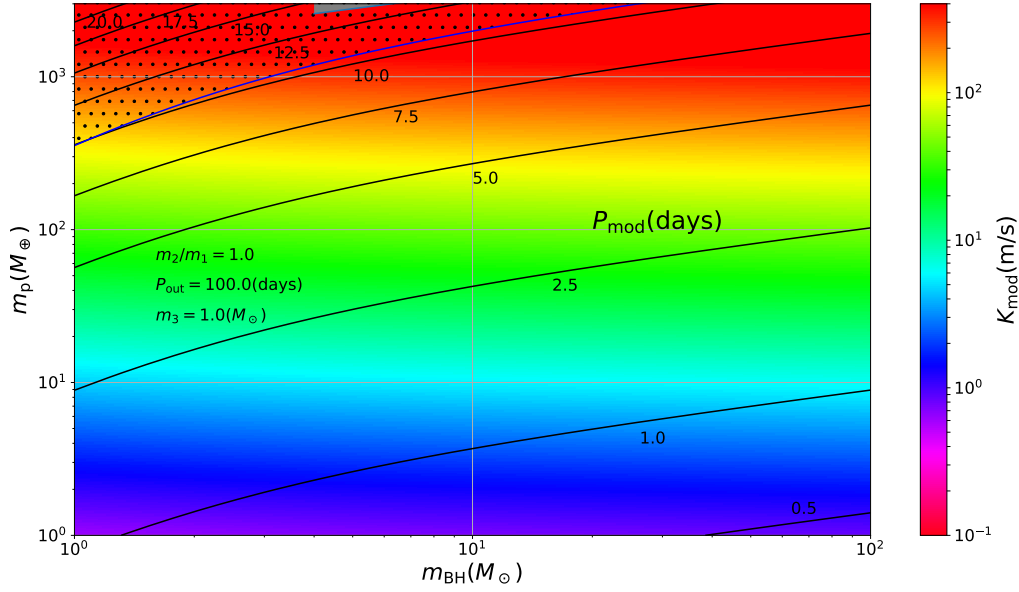


**Figure 8.** The relation between the masses of planet and inner binary with  $P_{\text{out}}$  fixed at 100 days. The  $P_{\text{mod}}$  denotes the period of the induced RV modulation, and  $K_{\text{mod}}$  is its amplitude. The dotted region excludes inner binary black-hole interpretation and the gray region excludes both interpretations.

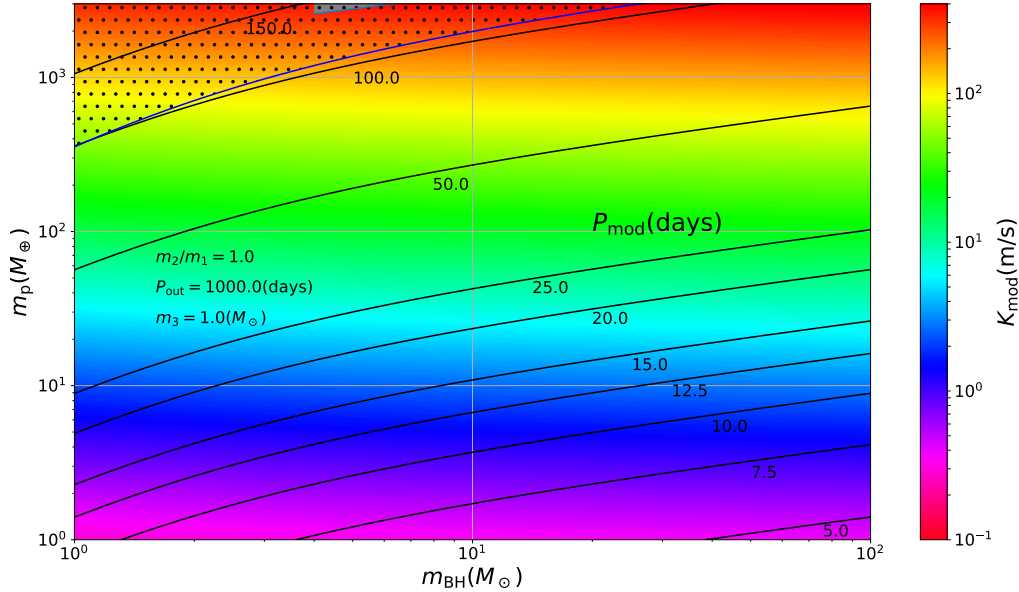


**Figure 9.** Same as Figure 8 but for  $P_{\text{out}}$  fixed at 1000 days.

For simplicity and definiteness, we have focused on a coplanar and near-circular three-body system and derived analytic perturbation formulae of the orbital elements for the outer body. We have confirmed the validity of our analytic formulae using numerical simulations.

As a specific example, we have considered the binary system 2M05215658+4359220 recently discovered by [Thompson et al. \(2018\)](#) in detail. From the observational uncertainties of the current radial velocity data of the outer red giant, we have derived constraints on the possible inner BBH of the system. If the central object inside the system is indeed a binary black hole with roughly equal masses, the current data exclude the inner binary with more than 12.5 day orbital period. Future RV follow-up observations of this system will either strengthen the constraint or even detect a signature of the inner BBH.

A planet orbiting around the outer star also induces the RV modulation from the inner BBH if the parameters of the two different pictures satisfy a couple of relations. The degeneracy may be broken only by a tiny difference that is described in our perturbation formulae in principle, while very challenging in practice.

Although our current study assumes a fairly idealized configuration, there are a couple of known systems that are consistent with the assumption, and more importantly, our current analytic model will provide a useful analytic constraint on the system parameter before performing intensive systematic parameter searches using numerical simulations. In reality, our analytic RV formula can be used to construct RV follow-up plans prior to the actual observing runs. This will be particularly useful because *Gaia* and *TESS* are expected to identify  $\sim 10^3$  binaries in the future.

We plan to generalize the current methodology for eccentric and non-coplanar systems. Finally, we emphasize that our current result may be applied to a broader class of objects in a three-body system, including a possible binary planet around a host star. We hope to report those developments elsewhere in due course.

## ACKNOWLEDGEMENTS

We thank Rosemary Mardling for very careful reading and numerous constructive comments, which significantly improved the early manuscript of this paper. We also thank Makiko Nagasawa, Re'em Sari, Alessandro Trani, and Anna Lisa Varri, for discussion on dynamical evolution of multi-body systems. The numerical simulation presented in this paper makes use of the public N-body code package *rebound*. Y.S. gratefully acknowledges the support from Grants-in Aid for Scientific Research by Japan Society for Promotion of Science (JSPS) No.18H01247 and No.19H01947, and from JSPS Core-to-core Program “International Network of Planetary Sciences”.

## REFERENCES

- Abbott B. P., et al., 2016, *Physical Review Letters*, **116**, 061102
- Barnes J. W., O’Brien D. P., 2002, *ApJ*, **575**, 1087
- Belczynski K., Kalogera V., Bulik T., 2002, *ApJ*, **572**, 407
- Belczynski K., Taam R. E., Kalogera V., Rasio F. A., Bulik T., 2007, *ApJ*, **662**, 504
- Belczynski K., Dominik M., Repetto S., Holz D. E., Fryer C. L., 2012, preprint, ([arXiv:1208.0358](https://arxiv.org/abs/1208.0358))
- Belczynski K., Holz D. E., Bulik T., O’Shaughnessy R., 2016, *Nature*, **534**, 512
- Bird S., Cholis I., Muñoz J. B., Ali-Haïmoud Y., Kamionkowski M., Kovetz E. D., Raccanelli A., Riess A. G., 2016, *Physical Review Letters*, **116**, 201301
- Breivik K., Chatterjee S., Larson S. L., 2017, *ApJ*, **850**, L13
- Danby J. M. A., 1988, *Fundamentals of celestial mechanics*. Willmann-Bell, Inc.
- Dominik M., Belczynski K., Fryer C., Holz D. E., Berti E., Bulik T., Mandel I., O’Shaughnessy R., 2012, *ApJ*, **759**, 52
- Dominik M., Belczynski K., Fryer C., Holz D. E., Berti E., Bulik T., Mandel I., O’Shaughnessy R., 2013, *ApJ*, **779**, 72
- El-Badry K., Rix H.-W., 2018, *MNRAS*, **480**, 4884
- Holman M. J., Wiegert P. A., 1999, *AJ*, **117**, 621
- Kawanaka N., Yamaguchi M., Piran T., Bulik T., 2017, in Gomboc A., ed., *IAU Symposium Vol. 324, New Frontiers in Black Hole Astrophysics*. pp 41–42, [doi:10.1017/S1743921316012606](https://doi.org/10.1017/S1743921316012606)
- Kinugawa T., Inayoshi K., Hotokezaka K., Nakauchi D., Nakamura T., 2014, *MNRAS*, **442**, 2963
- Kinugawa T., Miyamoto A., Kanda N., Nakamura T., 2016, *MNRAS*, **456**, 1093
- Mardling R. A., 2013, *MNRAS*, **435**, 2187
- Mardling R. A., Aarseth S. J., 2001, *MNRAS*, **321**, 398
- Mashian N., Loeb A., 2017, *MNRAS*, **470**, 2611
- Masuda K., Hotokezaka K., 2018, preprint, ([arXiv:1808.10856](https://arxiv.org/abs/1808.10856))
- Moulton F. R., 1914, *An introduction to celestial mechanics*. Dover Publications, Inc.
- Murray C. D., Dermott S. F., 2000, *Solar System Dynamics*. Cambridge University Press
- O’Leary R. M., Kocsis B., Loeb A., 2009, *MNRAS*, **395**, 2127
- Peters P. C., 1964, *Physical Review*, **136**, 1224
- Portegies Zwart S. F., McMillan S. L. W., 2000, *ApJ*, **528**, L17
- Ransom S. M., et al., 2014, *Nature*, **505**, 520
- Rein H., Tamayo D., 2015, *MNRAS*, **452**, 376
- Rodriguez C. L., Haster C.-J., Chatterjee S., Kalogera V., Rasio F. A., 2016, *ApJ*, **824**, L8
- Sasaki M., Suyama T., Tanaka T., Yokoyama S., 2016, *Physical Review Letters*, **117**, 061101
- Sasaki M., Suyama T., Tanaka T., Yokoyama S., 2018, *Classical and Quantum Gravity*, **35**, 063001
- Spera M., Mapelli M., Giacobbo N., Trani A. A., Bressan A., Costa G., 2019, *MNRAS*, **485**, 889
- Tagawa H., Umemura M., Gouda N., 2016, *MNRAS*, **462**, 3812
- Thompson T. A., et al., 2018, preprint, ([arXiv:1806.02751](https://arxiv.org/abs/1806.02751))
- Toonen S., Hamers A., Portegies Zwart S., 2016, *Computational Astrophysics and Cosmology*, **3**, 6
- Yamaguchi M. S., Kawanaka N., Bulik T., Piran T., 2018, *ApJ*, **861**, 21
- Ziegler C., et al., 2018, *AJ*, **156**, 259



symbol	value
$a_{\text{out}}$	2.0 au
$a_{\text{in}}$	0.1 au
$m_1$	10.0 $M_{\odot}$
$m_2$	10.0 $M_{\odot}$
$m_3$	0.5 $M_{\odot}$
$e_{\text{in}}$	$10^{-8}$
$e_{\text{out}}$	$10^{-5}$
$f_{\text{in}}$	$\pi/6$
$f_{\text{out}}$	$2\pi/3$
$\varpi_{\text{in}}$	0.0
$\varpi_{\text{out}}$	0.0

**Table A1.** Initial condition for numerical simulation described in Appendix A

## APPENDIX A: COMPARISON OF THE PERTURBATION SOLUTION WITH NUMERICAL SIMULATION

In this appendix, we consider the validity and limitation of the perturbative approximation formulae derived in section 3 by comparing equations (3.1)–(3.4) and the radial velocity against the result of numerical simulation based on a public N-body package *rebound*. In this numerical simulation, we choose WHfast integrator, which is one of the fast and accurate symplectic integrators (Rein & Tamayo 2015), and we fix time step at  $10^{-6}$  yr/ $2\pi$ .

This section focuses on a system with  $\alpha \ll 1$  and  $m_3 \ll m_1 + m_2$  whose parameters are summarized in Table A1.

Consider first the orbital elements. Figure A1 (a) – (c) show the comparison for  $a_{\text{out}}/a_{\text{out}}^{(i)} - 1$ ,  $\cos \lambda_{\text{out}}$ ,  $h_{\text{out}} - h_{\text{out}}^{(i)}$  and  $k_{\text{out}} - k_{\text{out}}^{(i)}$ , respectively. As mentioned in section 3, since the short-term oscillations reflected in  $V_{\text{binary}}$  are the direct evidence of the inner binary, we also check the corresponding short-period terms  $h_{\text{out,short}}$  and  $k_{\text{out,short}}$  in  $h_{\text{out}}$  and  $k_{\text{out}}$ :

$$h_{\text{out,short}} \equiv \frac{m_1 m_2}{m_{12}^2} \alpha^2 \left[ -\frac{3}{8(2\nu_{\text{in}}^{(i)} - \nu_{\text{out}}^{(i)})} S_0[(2\nu_{\text{in}}^{(i)} - \nu_{\text{out}}^{(i)})t + (2\epsilon_{\text{in}}^{(i)} - \epsilon_{\text{out}}^{(i)})] + \frac{21}{8(2\nu_{\text{in}}^{(i)} - 3\nu_{\text{out}}^{(i)})} S_0[(2\nu_{\text{in}}^{(i)} - 3\nu_{\text{out}}^{(i)})t + (2\epsilon_{\text{in}}^{(i)} - 3\epsilon_{\text{out}}^{(i)})] \right] \quad (\text{A1})$$

and

$$k_{\text{out,short}} \equiv \frac{m_1 m_2}{m_{12}^2} \alpha^2 \left[ -\frac{3}{8(2\nu_{\text{in}}^{(i)} - \nu_{\text{out}}^{(i)})} C_0[(2\nu_{\text{in}}^{(i)} - \nu_{\text{out}}^{(i)})t + (2\epsilon_{\text{in}}^{(i)} - \epsilon_{\text{out}}^{(i)})] - \frac{21}{8(2\nu_{\text{in}}^{(i)} - 3\nu_{\text{out}}^{(i)})} C_0[(2\nu_{\text{in}}^{(i)} - 3\nu_{\text{out}}^{(i)})t + (2\epsilon_{\text{in}}^{(i)} - 3\epsilon_{\text{out}}^{(i)})] \right]. \quad (\text{A2})$$

The results are shown in Figures A2 and A3.

In what follows, we use the subscripts app and sim to denote the quantities from approximation formulae and numerical simulation, respectively. The upper panel of Figure A1 (a) shows that the fractional modulation amplitude of  $a_{\text{out}}$  relative to  $a_{\text{out}}^{(i)} - 1$  is  $O(10^{-5})$ . The difference between our analytic solution and the numerical result plotted in the lower panel is about 5 percent of the modulation. The periodic signal at the frequency  $2\nu_{\text{in}}$  is also gradually modulated with the frequency  $\nu_{\text{out}}$ .

Figure A1 (b) and (c) indicate that  $\cos \lambda_{\text{out}}$ ,  $h_{\text{out}}$  and  $k_{\text{out}}$  exhibit the very similar behavior, while their fractional residual amplitudes are significantly smaller than that of  $a_{\text{out}}$ .

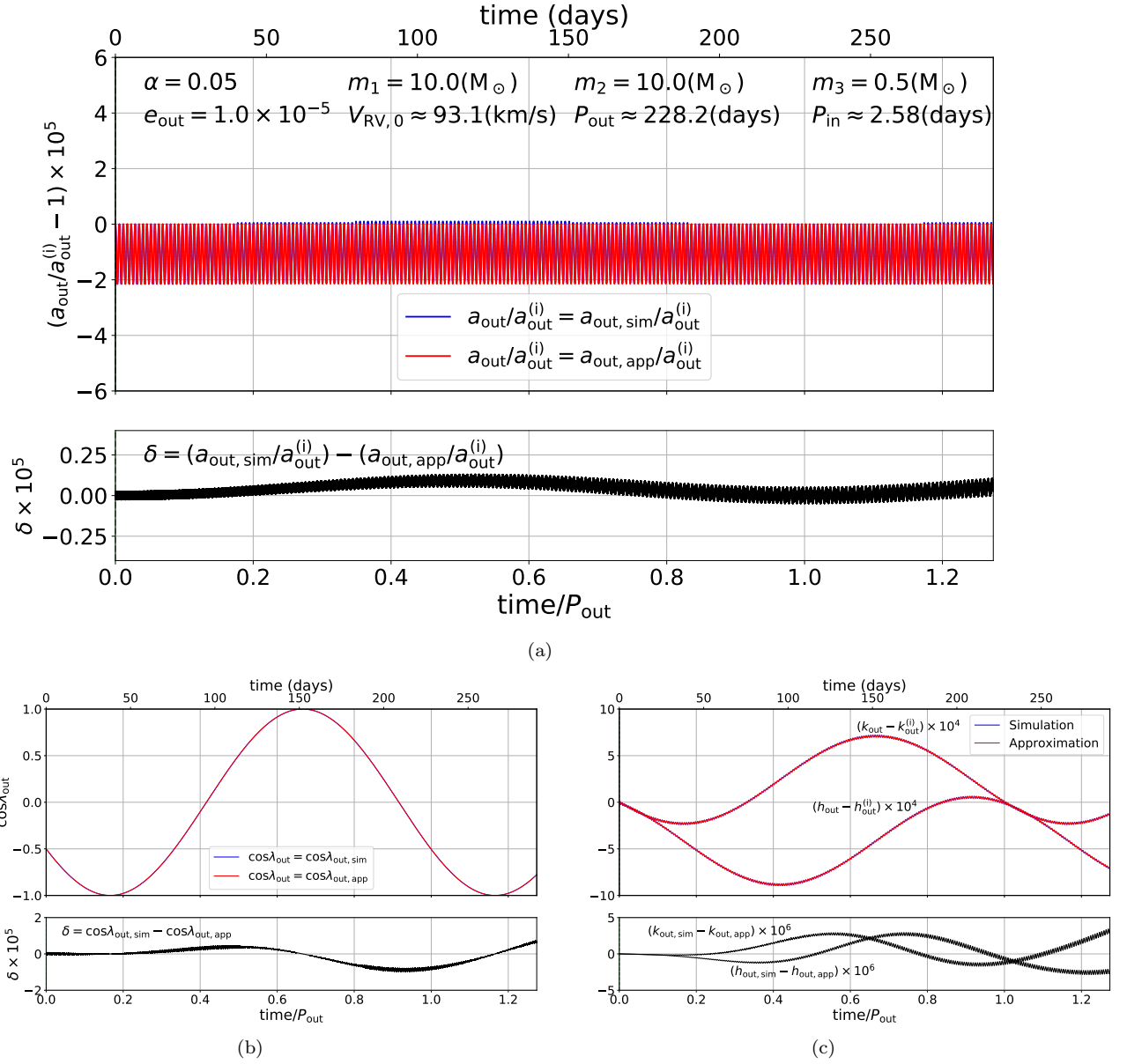
Figure A2 and A3 show the comparison for short-term oscillations  $h_{\text{out,short}}$  and  $k_{\text{out,short}}$ , indicating that the fractional deviation of those amplitudes is about 3% at  $t \approx P_{\text{out}}$  although  $h_{\text{out}}$  and  $k_{\text{out}}$  deviates gradually due to the long-term modulation.

Consider next the comparison of the RV. Figure A4 compares  $V_{\text{Kep1,app}}$  (see Table 3) with  $V_{\text{RV,sim}}$ . As we can see in Figure A4, while the major component of the RV can be explained by  $V_{\text{Kep1}}$ , the residual shows the presence of the other modes, *i.e.*  $V_{\text{Kep2}}$  to  $V_{\text{binary4}}$  in Table 3. Among the modes in the residual, the short-term oscillations corresponding to  $V_{\text{binary}}$  include the information of the inner binary.

Figure A5 compares  $V_{\text{binary,app}}$  (see Table 3) with  $V_{\text{RV,sim}} - (V_{\text{Kep,app}} + V_{\text{ecc,app}})$ . The spikes in Figure A5 correspond to the short-term spikes in the residual of Figure A4. The  $V_{\text{binary}}$  from approximation shows significant deviation after about  $0.4P_{\text{out}}$ , however, the amplitude of each spike only deviates about 4% at  $t \approx P_{\text{out}}$ . Figure A6 shows the same plot as Figure A5 for longer time. It shows that the approximation formula is no longer accurate after a long time from the initial epoch due to the long-term modulation. However, the amplitude of each spike only deviates about 8% at  $t \approx 3.5P_{\text{out}}$ .

Figures A1 to A8 confirm that our approximation formulae are sufficiently accurate as long as both  $\alpha$  and eccentricities are small enough. Even though the longer-term modulation starts to dominate the entire amplitude of the signals, the higher-frequency component of the RV that carries the information of the inner binary can be reproduced by our analytic solution within a few percent; see Figure A5 and A6. Since we consider to detect a binary black hole from several periods of short-term modes in whole RV, the long-term accuracy is not required. Therefore, the long-term error, if exists, would not matter practically.

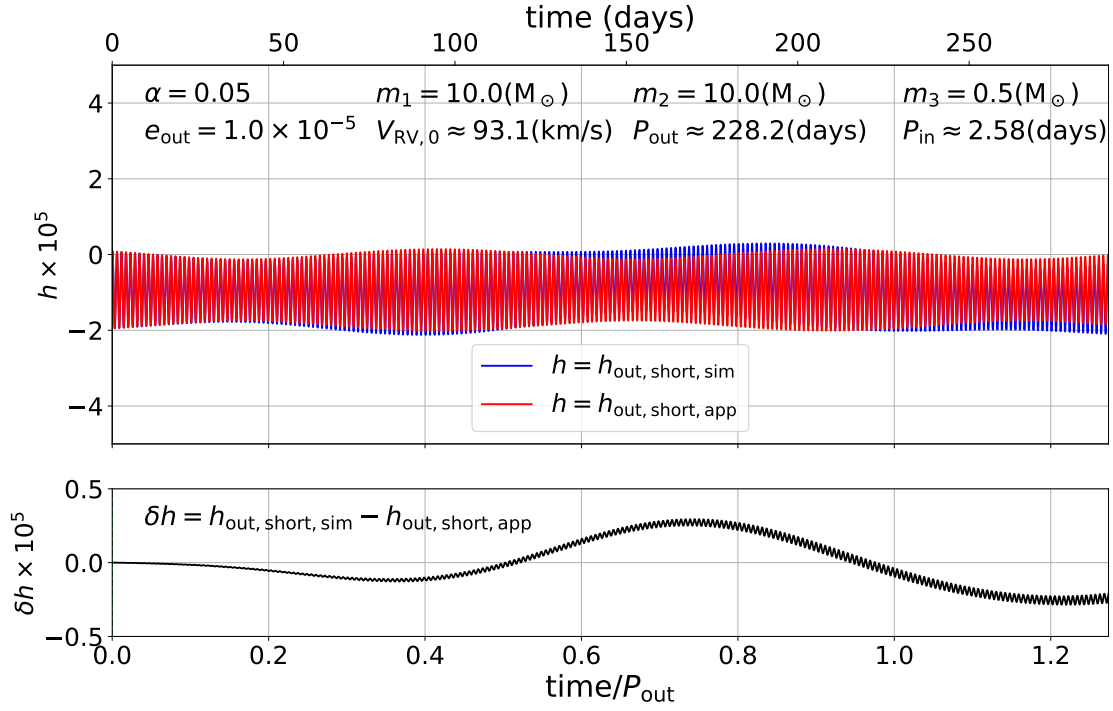
In order to prove that the lower-frequency modulation does not affect the accuracy of the RV components around at



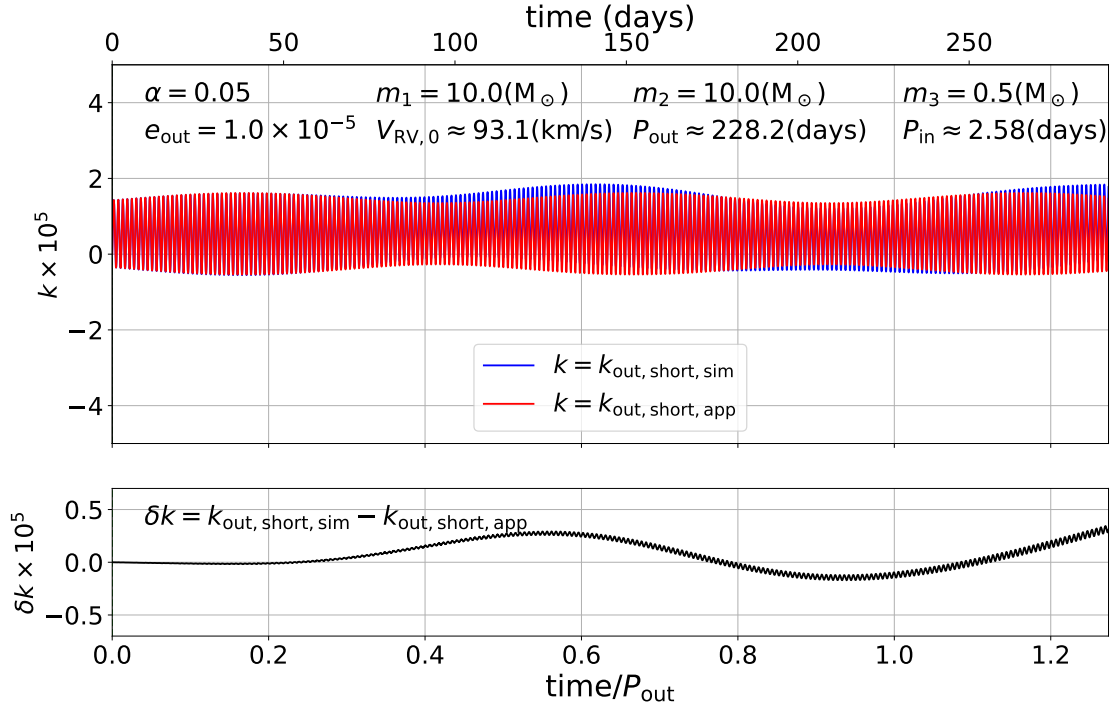
**Figure A1.** Comparison of our approximate formulae against numerical simulation for the initial condition summarized in Table A1: (a)  $a_{\text{out}}/a_{\text{out}}^{(i)} - 1$ , (b)  $\cos \lambda_{\text{out}}$ , and (c)  $h_{\text{out}} - h_{\text{out}}^{(i)}$  and  $k_{\text{out}} - k_{\text{out}}^{(i)}$

frequency  $2\nu_{\text{in}}$ , we plot Figure A7 and A8 that are renormalized adopting the values of all variables at  $t = 3P_{\text{out}}$  as their initial values. They show that the higher-frequency components in our analytic solutions remain accurate at least for a few orbital periods of the outer binary if they are reset at any arbitrary epoch.

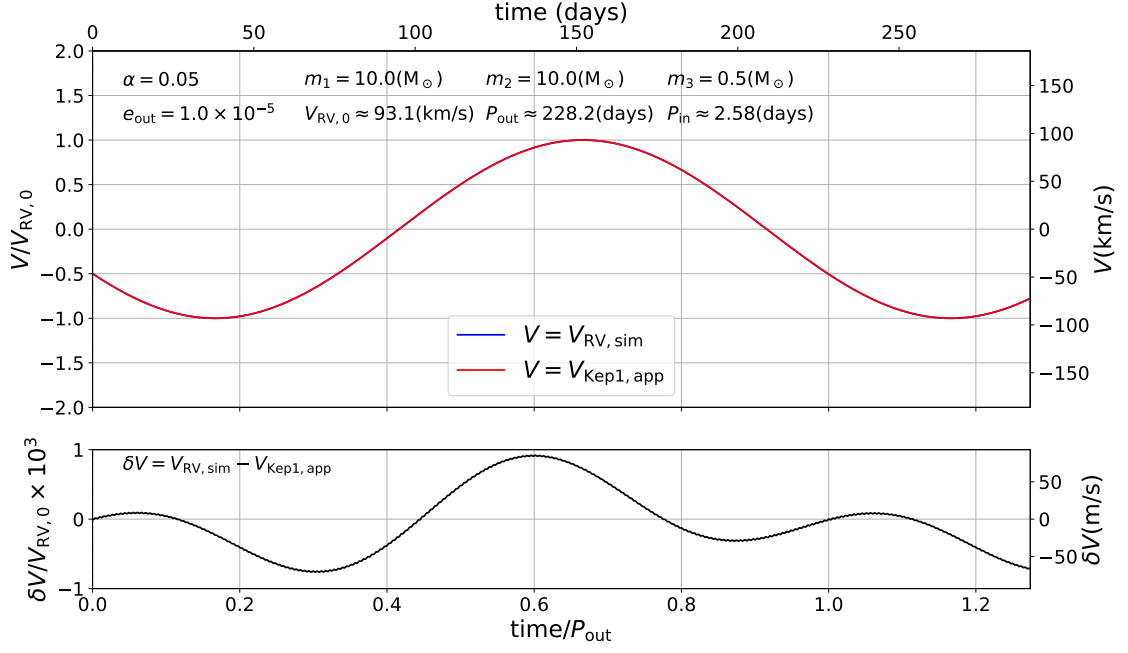
This paper has been typeset from a  $\text{T}_{\text{E}}\text{X}/\text{L}_{\text{A}}\text{T}_{\text{E}}\text{X}$  file prepared by the author.



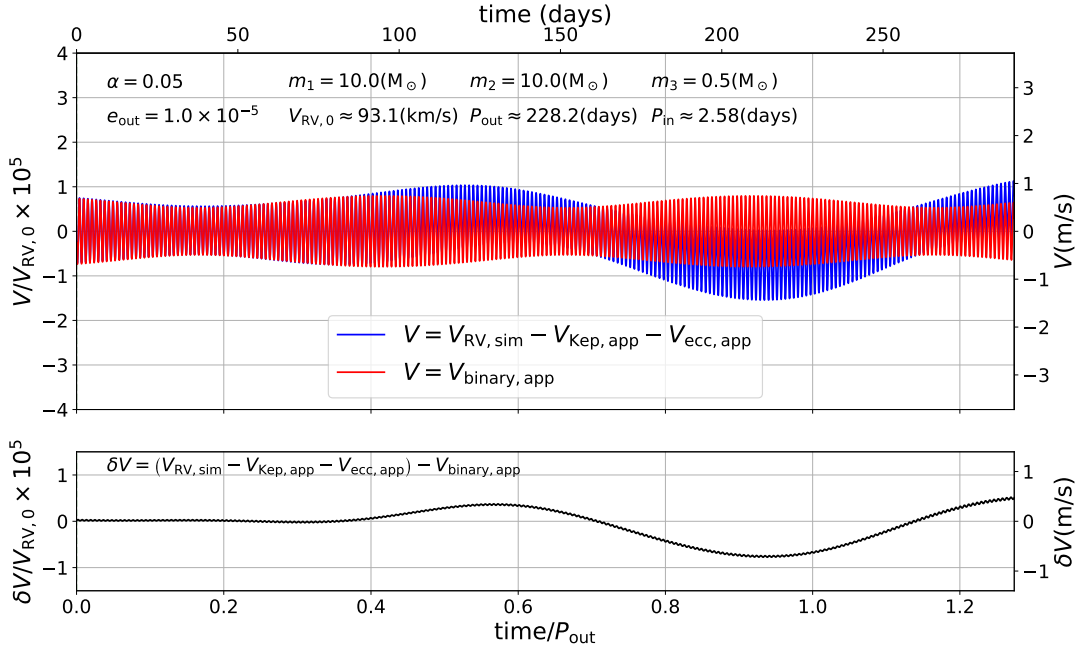
**Figure A2.** Comparison of  $h_{\text{out, short, sim}} \equiv h_{\text{out, sim}} - (h_{\text{out, app}} - h_{\text{out, short, app}})$  and  $h_{\text{out, short, app}}$  (see equation (A1)) for the initial condition listed in Table A1



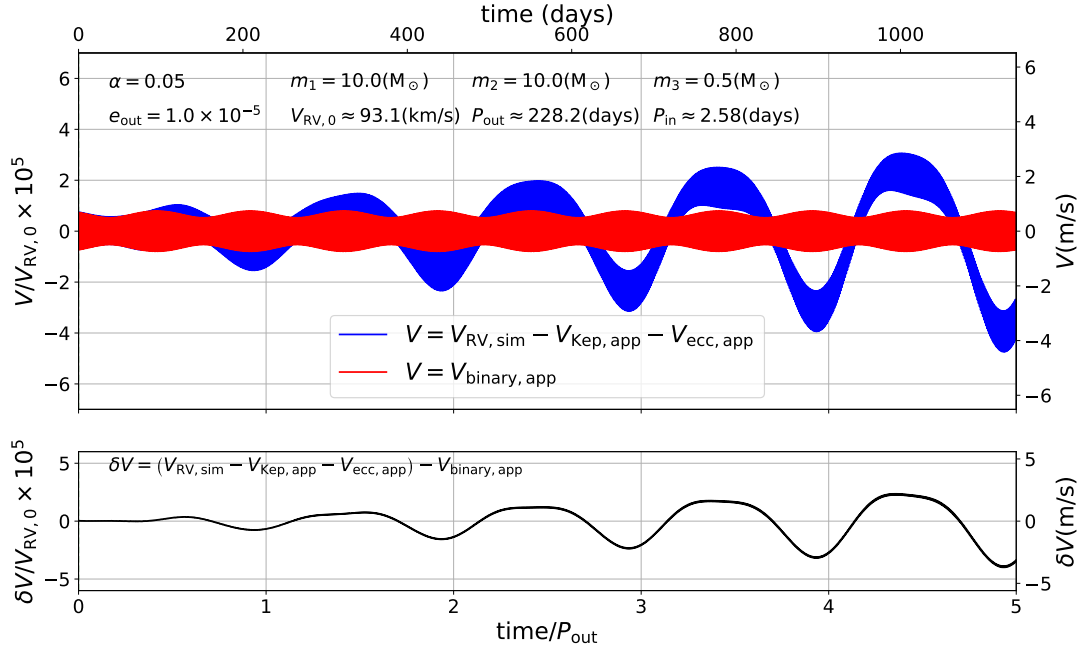
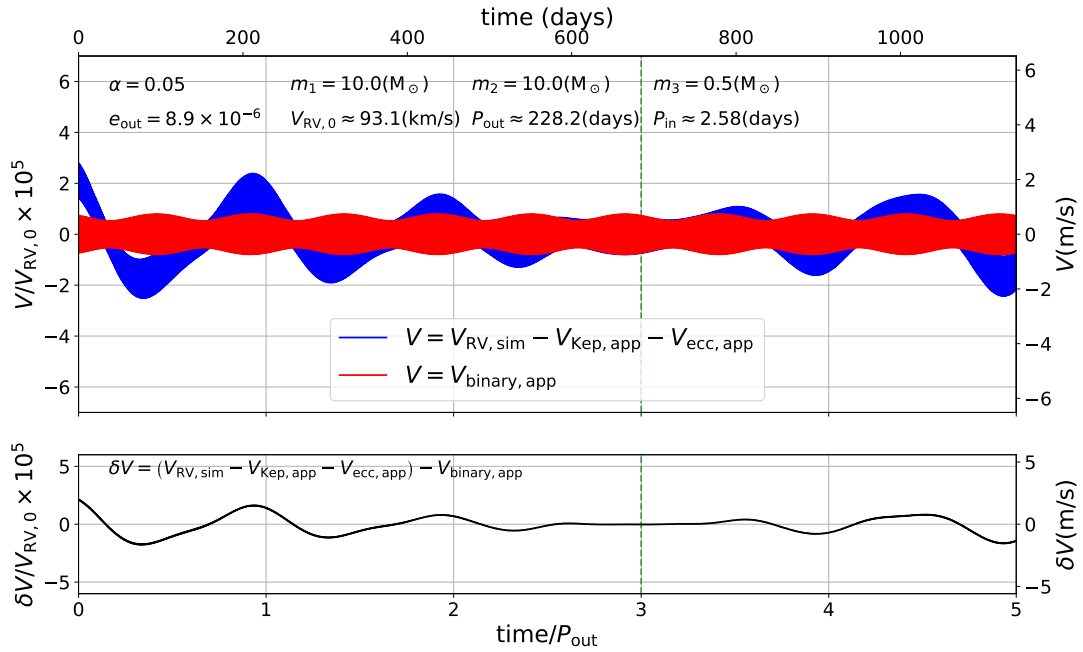
**Figure A3.** Comparison of  $k_{\text{out, short, sim}} \equiv k_{\text{out, sim}} - (k_{\text{out, app}} - k_{\text{out, short, app}})$  and  $k_{\text{out, short, app}}$  (see equation (A2)) for the initial condition listed in Table A1



**Figure A4.** Comparison of  $V_{RV, sim}$  and  $V_{Kep1, app}$  (Table 3) for the initial condition summarized in Table A1



**Figure A5.** Same as Figure A4 but for  $V_{RV, sim} - (V_{Kep, app} + V_{ecc, app})$  and  $V_{binary, app}$  (see Table 3)

**Figure A6.** Same as Figure A5 but for  $0 \leq t \leq 5P_{out}$ **Figure A7.** Same as Figure A6 but we adopt the analytic formulae using the orbital parameters at  $t = 3P_{out}$  for their initial values.

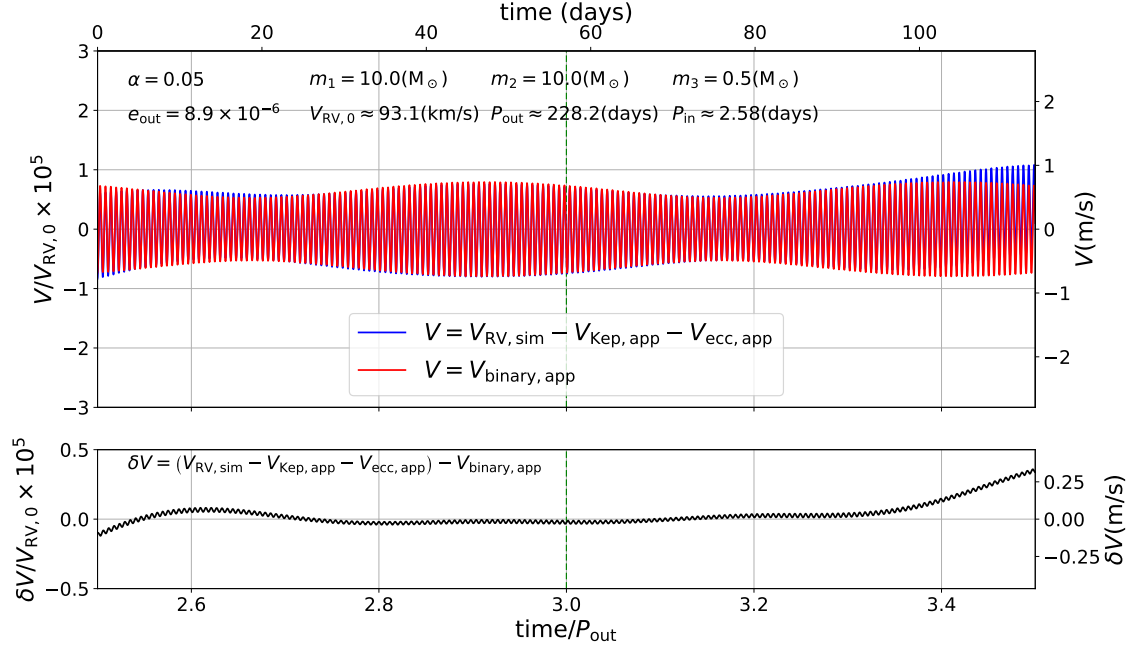


**Figure A8.** An enlarged version of Figure A7 for  $2.5P_{out} \leq t \leq 3.5P_{out}$